IOPscience iopscience.iop.org

Home Search Collections Journals About Contact us My IOPscience

Probe measurements of electron-energy distributions in plasmas: what can we measure and how can we achieve reliable results?

This article has been downloaded from IOPscience. Please scroll down to see the full text article.

2011 J. Phys. D: Appl. Phys. 44 233001

(http://iopscience.iop.org/0022-3727/44/23/233001)

View the table of contents for this issue, or go to the journal homepage for more

Download details:
IP Address: 134.131.125.50
The article was downloaded on 21/06/2011 at 19:52

Please note that terms and conditions apply.

IOP PUBLISHING JOURNAL OF PHYSICS D: APPLIED PHYSICS

J. Phys. D: Appl. Phys. **44** (2011) 269501 (1pp) doi:10.1088/0022-3727/44/26/269501

Corrigendum

Probe measurements of electron-energy distributions in plasmas: what can we measure and how can we achieve reliable results?

V A Godyak and V I Demidov 2011 *J. Phys. D: Appl. Phys.* **44** 233001

Received 31 May 2011
Published 16 June 2011

On page 4 in equations (4) and (5) as well as in the first line in the right column, 'f_0' should be replaced by 'f'.

On page 4, equation (9) should be replaced by

$$\frac{\mathrm{d}^2 I_e}{\mathrm{d}V^2} = \frac{2\pi e^3 S_p}{m^2} f_0(eV) = -\frac{e^2 S_p}{4}\sqrt{\frac{2e}{mV}} F(eV)$$
$$= \frac{e^3 S_p}{2\sqrt{2m}} f_p(eV).$$

On page 5, equation (11) should be replaced by

$$T_e = \frac{4\sqrt{2m/|e|}}{3NS_p} \int_0^{-\infty} I_e''(V)|V|^{3/2}\mathrm{d}V.$$

 © 2011 IOP Publishing Ltd Printed in the UK & the USA

IOP PUBLISHING — JOURNAL OF PHYSICS D: APPLIED PHYSICS

J. Phys. D: Appl. Phys. **44** (2011) 233001 (30pp) doi:10.1088/0022-3727/44/23/233001

TOPICAL REVIEW

Probe measurements of electron-energy distributions in plasmas: what can we measure and how can we achieve reliable results?

V A Godyak[1] **and V I Demidov**[2]

[1] RF Plasma Consulting, Brookline, MA 02446, USA
[2] Department of Physics, West Virginia University, Morgantown, WV 26506, USA

Received 8 April 2011
Published 16 May 2011
Online at stacks.iop.org/JPhysD/44/233001

Abstract

An electric-probe method for the diagnostics of electron-distribution functions (EDFs) in plasmas is reviewed with emphasis on receiving reliable results while taking into account appropriate probe construction, various measurement errors and the limitations of theories. The starting point is a discussion of the Druyvesteyn method for measurements in weakly ionized, low-pressure and isotropic plasma. This section includes a description of correct probe design, the influence of circuit resistance, ion current and plasma oscillations and probe-surface effects on measurements. At present, the Druyvesteyn method is the most developed, consistent and routine way to measure the EDF. The following section of the review describes an extension of the classical EDF measurements into higher pressures, magnetic fields and anisotropic plasmas. To date, these methods have been used by a very limited number of researchers. Therefore, their verification has not yet been fully completed, and their reliable implementation still requires additional research. Nevertheless, the described methods are complemented by appropriate examples of measurements demonstrating their potential value.

(Some figures in this article are in colour only in the electronic version)

Nomenclature

a	probe radius
A, A_n	instrumental functions
b	probe-holder radius
$\boldsymbol{B}$	vector of the magnetic field ($\lvert\boldsymbol{B}\rvert = B$)
C	filter capacitance
C_{in}	input capacitance
C_{pr}	capacitance of probe referenced to plasma
C_q	coefficient defying class of EEDF
C_0	winding stray capacitance
D_a	ambipolar diffusion coefficient
D_e	diffusion coefficient of electrons
e	electron charge (-1.6×10^{-19} C)
f	electron-distribution function (EDF)
F	electron-energy distribution function
f_j^k	tensor component of the EDF ($f_j \equiv f_j^0$)
f_{fl}	typical fluctuation time
f_p	electron-energy probability function
f_{pm}	measured electron-energy probability function
$f_0, \vec{f}_1$	isotropic and directed parts of the EDF ($\lvert\vec{f}_1\rvert = f_1$)
G	gain
I_B	Bohm current to counter-electrode
I_c	displacement current
I_d	discharge current
I_e	electron probe current ($I_e' = dI_e/dV$, $I_e'' = d^2I_e/dV^2$)
I_{eo}	electron probe saturation current

 © 2011 IOP Publishing Ltd Printed in the UK & the USA

I_p probe current ($I'_p = dI_p/dV$, $I''_p = d^2I_p/dV^2$)
I_r maximal current provided by the reference counter-electrode
I_z current corresponding generation of electrons in plasma volume
K number of probe orientations
l probe length
L inductance
L_f rf-filter inductance
m electron mass
M ion mass
M_H mass of hydrogen ion
N plasma density
N_m measured plasma density
N_s plasma density near chamber wall
N_0 plasma density at volume centre
P_j Legendre polynomial ($P_j \equiv Y_j^0$)
Q Q-factor
$\vec{r}$ space-coordinate vector
R_c probe circuit resistance
R_{csh} chamber sheath resistance
R_{ext} external resistance (includes all resistances between probe tip and voltage source)
R_f rf-filter resistance
R_{int} internal resistance (includes R_{csh}, R_x and R_{pl})
R_{Le} electron Larmor radius
R_{pl} probe presheath resistance
R_{po} minimal value of probe-sheath resistance
R_{psh} probe-sheath resistance
R_t contact resistance
R_x contaminated chamber surface resistance
R_w resistance of lead wires
R_ν sensor resistance
S_{ch} plasma chamber surface area
S_p area of the probe surface
t time
T_e electron temperature (in units of energy)
T_{el} low-energy electron temperature in bi-Maxwellian EEDF
T_{em} measured electron temperature (in units of energy)
T_{esc} electron screening temperature (in units of energy)
T_g gas temperature
T_{he} high-energy electron temperature in bi-Maxwellian EEDF
$\vec{v}$ vector of the electron velocity ($|\vec{v}| = v$)
V probe voltage with respect to the plasma
V_a probe voltage referenced to ground
v_b ion sound (Bohm) speed ($v_B = (T_e/M)^{1/2}$)
V_{dc} dc voltage
V_{fl} voltage of floating probe
V_{ext} voltage drop across external resistor
V_{int} voltage drop across internal resistor
V_{prf} rms rf plasma potential referenced to ground
V_r residual voltage
V_s plasma-space potential
V_{shfr} rms rf voltage in probe sheath
V_{sw} voltage range of a sweep
V_t voltage of small, time-variable amplitude
X_f rf-filter reactance
Y_j^k spherical functions
Z_f filter impedance
Z_{pr} impedance between probe and plasma

Greek symbols

γ geometrical factor
Γ_e generation rate of electrons
δ $=R_c/R_{po}$
ε kinetic energy of electrons
ε^* atom (molecule) excitation energy
$\langle\varepsilon\rangle$ average electron energy ($\langle\varepsilon\rangle = (3/2)T_e$)
ϑ polar angle in the spherical coordinate system
θ' polar angle in equation (24)
λ angle between axis of cylindrical probe and symmetry axis of plasma
λ_e mean free path of electrons
Λ plasma characteristic (diffusion) length
Λ_p probe diffusion length
λ_D electron Debye radius
λ_ε electron-energy relaxation length
λ_i mean free path of ions
ν frequency of electron–neutral collisions
ν_{ee} frequency of interelectron collisions
τ_D time scale for electron diffusion to probe
τ_e electron transient time across probe sheath
τ_i ion transient time across probe sheath
τ_p plasma transient time
τ_{pN} plasma density decay time in afterglow
τ_s probe scan time
τ_{sw} sweep time
φ azimuthal angle in a spherical coordinate system
ϕ plasma potential
Φ_f, Φ_c angles defining orientation of probe in plasma
Ψ_s sink parameter
Ψ diffusion parameter
ω rf frequency
ω_e electron-plasma frequency
ω_i ion-plasma frequency
ω_H electron cyclotron frequency

Abbreviations

dc direct current
rf radio frequency
CCP capacitive coupled plasma
CW continuous wave
ECR electron cyclotron resonance
EDF electron-distribution function
EEDF electron-energy distribution function
EEPF electron-energy probability function
hf high frequency

ICP inductive coupled plasma
MP measurement probe
OD outer diameter
PVS probe-voltage source
RVS residual voltage source
RP reference probe

1. Introduction

An electric probe is essentially a conducting object immersed into or facing (as in the case of a wall probe) plasma for the purpose of diagnostics. The first, not particularly successful attempts to use floating electric conductors for the measurement of plasma-space potentials V_s were made at the beginning of the 20th century (see, e.g., [1]), but the first real progress in obtaining plasma parameters from probe measurements was made later by Langmuir *et al* [2, 3]. Therefore, these probes are commonly referred to as Langmuir probes.

Langmuir demonstrated that, for spherical and cylindrical probes inserted into a weakly ionized low-pressure plasma in which the dimension of the plasma volume distorted by the probe is significantly smaller than the mean free path of the electrons λ_e (i.e. electrons from the undisturbed plasma can reach the probe surface without collisions), the application of a voltage V to the probe and the measurement of the probe current I_p can provide reliable information about not only V_s but also the plasma density N and the electron temperature T_e. The theory developed by Langmuir led to the next important step in the development of probe diagnostics, which was undertaken by Druyvesteyn [4], who demonstrated that the second derivative of the probe current with respect to the probe potentials $d^2I_p/dV^2 \equiv I_p''$ allows the determination of the electron-energy distribution function (EEDF) in the plasma.

The electric probe was seen as a rather simple and attractive scientific instrument, and after seminal works by Langmuir and Druyvesteyn, numerous probe measurements in gas-discharge plasmas have been conducted by many authors. Today, the field of electric probes is enormous, and many works on the subject can be found in the literature (see, e.g., the reviews and books [5–27] and references therein). Druyvesteyn method has been used for measurements of EEDFs in dc plasma of positive column in noble and molecular gases [5], including striations [28]; plasma near anode [29] and cathode [30]; hollow cathode plasma [31]; afterglow [32]; photoplasma [33]; plasma with negative ions [34, 35] and in many other papers (see above reviews and monographs). Since the time of Langmuir and Druyvesteyn, probe theory has been extended dramatically, allowing the diagnostics of different types of plasmas, including those experiencing high pressure, strong magnetic fields and anisotropy. More sophisticated probe constructions (some of which can hardly be considered as Langmuir probes) allow measurements in chemically active plasmas (e.g. by a heated probe [12, 24, 25, 36]) and under the harsh condition of fusion-related plasmas (reciprocating probe [37]). Currently, electric probes can measure not only the basic plasma parameters, such as N, T_e, V_s and EEDF, but, depending on the plasma type, can also measure other fluid observables, such as the flow velocities of ions (Mach probe [20, 25]), ion temperatures (ion-sensitive probe [25, 38]) and oscillations of N, T_e, V_s in magnetized plasma (magnetically insulated baffled (MIB) probes [39] such as Katsumata probes [38, 40], plug probes [41, 42], baffled probes [43, 44], tunnel probes [45] and ball-pin probes [46]). The potential of the electric-probe method has not been yet fully exploited and has great possibilities for development.

Despite the development of new probe constructions and theories, which are useful for many specific applications and branches of plasma physics, simple cylindrical Langmuir probes are currently the main contact diagnostic tool for measuring plasma parameters in weakly ionized, low-pressure plasmas in both applied and basic plasma research. For non-equilibrium plasmas with non-Maxwellian electron-energy distributions, the measurement of the EEDF is a unique way to obtain the basic plasma parameters and the rates of plasma-chemical processes without assuming a Maxwellian EEDF, instead using the corresponding integrals of the EEDFs measured experimentally.

However, the interpretation of the measurements for even this simple case can be intricate and confusing. Therefore, it is not surprisingly that erroneous results and incorrect applications of Langmuir probes are common in the literature. The errors mainly arise from the poor design of probe experiments, incorrect probe constructions and circuit designs and a lack of awareness of possible error sources. Sometimes, the applicability and limitations of probe theories used for the evaluation of plasma parameters are ignored. Although these issues have been considered in many probe reviews and in specific review of EEDF measurements [19], many recent papers on EEDF measurements leave these problems unaddressed. At the same time, for the last twenty years after the publication of review [19], there has been significant progress in probe experimental design, effectively addressing the aforementioned problems mainly in relation to rf plasmas typical for plasma-processing reactors.

The purpose of the present review is to analyse the most common sources of error in EEDF measurements and possible ways to avoid them by proper design of the probe experiment. Additionally, we consider recent developments of EEDF measurements in complicated plasma conditions. Among them are measurements in time-variable, collisional, magnetized and anisotropic plasmas and electron-spectroscopy analysis. We also present numerous examples of EEDF measurements obtained with laboratory and commercial probe instruments in which possible sources of errors were adequately addressed. In many aspects, the present review summarizes the authors' experiences gained over decades of practicing and developing probe diagnostics.

The paper is structured as follows. In the next section, we briefly describe the most detailed information that can be obtained from the probe measurements, namely the electron-distribution function, EDF and its derivatives, such as the EEDF. We also provide the primary formula for the Druyvesteyn method suitable for measurements in weakly ionized, low-pressure and isotropic plasma. Section 3 deals with the main sources of error in the probe measurements

and their mitigation. Section 4 demonstrates principles of the probe-diagnostics method beyond the limitations of the Druyvesteyn procedure, such as EEDF measurement in collisional, isotropic or magnetized plasmas and electron-spectroscopy diagnostics. The last chapter of this work provides concluding remarks.

2. General considerations

2.1. What we are going to measure

Electron gas in plasma is described by the electron-distribution function (EDF) $f(t, \vec{r}, \vec{v})$, where $\vec{r}$ is the space-coordinate vector and $\vec{v}$ is the velocity vector [47, 50]. The function gives the number of electrons in the volume element $d^3\vec{r} = dx \times dy \times dz$ having velocities between $\vec{v}$ and $\vec{v} + d\vec{v}$ at time t. This function can be used for the description of all kinetic processes with electron participation, including electron transport and the excitation of atoms and molecules in both isotropic and anisotropic plasmas. The electron density can be found from the function as

$$N(t, \vec{r}) = \int_{\vec{v}} f(t, \vec{r}, \vec{v})\, d\vec{v}. \tag{1}$$

In practice, it is convenient to express the EDF as a series [47],

$$f(t, \vec{r}, \vec{v}) = \sum_{j=0}^{\infty} \sum_{k=-j}^{j} f_j^k(t, \vec{r}, v) Y_j^k(\vartheta, \varphi), \tag{2}$$

where $v = |\vec{v}|$ is the electron speed, f_j^k are tensor components of the EDF, Y_j^k are spherical functions (harmonics), and ϑ and φ are polar and azimuthal angles in a spherical coordinate system. In many cases, due to electron collisions with molecules and plasma boundaries, the EDF is nearly symmetrical and can be represented by the two-term approximation

$$f(t, \vec{r}, \vec{v}) = f_0(t, \vec{r}, v) + \frac{\vec{v}}{v} \cdot \vec{f}_1(t, \vec{r}, v). \tag{3}$$

This representation is valid even for rather low gas pressures because most electrons are imprisoned in the plasma volume due to the near-wall sheath. Therefore, the two-term approximation is generally accepted in most plasma research. In some special cases (e.g. for very low pressures, strong electric fields and electron beams), the two-term approximation is not enough and the above expansion to spherical harmonics (general case) or to Legendre polynomials P_j for cylindrical symmetry (in this case, $k = 0$ and $P_j \equiv Y_j^0$) should be used.

In line with the EDF, the use of the EEDF, $F(t, \vec{r}, \varepsilon)$, which gives a number of electrons in the volume element having energies between ε and $\varepsilon + d\varepsilon$ (losing information about angle distribution), is generally accepted. For an isotropic EDF, $f(t, \vec{r}, \vec{v}) = f_0(t, \vec{r}, v)$ and, taking into account that $v = \sqrt{2\varepsilon/m}$, where ε is the electron kinetic energy and m is the electron mass, the following expression holds:

$$F(t, \vec{r}, \varepsilon) = 4m^{-3/2}\sqrt{2}\pi\sqrt{\varepsilon} f_0(t, \vec{r}, \sqrt{2\varepsilon/m}). \tag{4}$$

In this case, functions f_0 and F have identical information about the properties of the electron gas because the angular distribution for electrons is the same in any direction. Consequently, in the isotropic plasma, the electron density can be found as the following (omitting coordinates and time):

$$N = \int_0^{\infty} F(\varepsilon)\, d\varepsilon = 4m^{-3/2}\sqrt{2}\pi \int_0^{\infty} \sqrt{\varepsilon} f_0(\varepsilon)\, d\varepsilon. \tag{5}$$

The function $4m^{-3/2}\sqrt{2}\pi f_0(\varepsilon) = F(\varepsilon)/\sqrt{\varepsilon} \equiv f_p(\varepsilon)$ is frequently referred to as the electron-energy probability function (EEPF) [19, 48–50]. For isotropic plasma, it has the same information about the electron gas as EDF or EEDF and is frequently used to represent measured probe data. The EEPF, presented in a semi-log scale, allows the quick visualization of a departure of the measured EEPF from a Maxwellian distribution, which is a straight line in this representation. Note that some authors use different normalizations of the above distribution functions, but we believe that the representation given above is the most convenient way to read numerous published probe records. Knowledge of the EEDF or EEPF allows the calculation of the plasma parameters and the rates of plasma-chemical processes. Thus, for plasma density N and effective electron temperature T_e (defined for non-Maxwellian EEDF as a measure of the average electron energy $\langle\varepsilon\rangle$ as $T_e = (2/3)\langle\varepsilon\rangle$), the following expressions hold:

$$N = \int_0^{\infty} \sqrt{(\varepsilon)} f_p(\varepsilon)\, d\varepsilon, \tag{6}$$

and

$$T_e = \frac{2}{3} N^{-1} \int_0^{\infty} \varepsilon^{3/2} f_p(\varepsilon)\, d\varepsilon = \frac{2}{3} N^{-1} \int_0^{\infty} \varepsilon F(\varepsilon)\, d\varepsilon. \tag{7}$$

Similarly, the collision frequencies for electron–atom elastic collisions, excitation and ionization frequencies and the electron screening temperature T_{esc} can be calculated as appropriate integrals of the measured EEPF [51].

2.2. The Druyvesteyn method

Probe measurement of EEDF/EEPF in weakly ionized, low-pressure, isotropic plasma is based on the Langmuir expression for electron probe current [2, 3],

$$\begin{aligned} I_e &= \frac{2\pi e S_p}{m^2} \int_{eV}^{\infty} (\varepsilon - eV) f_0(\varepsilon)\, d\varepsilon \\ &= \frac{e S_p}{2\sqrt{2m}} \int_{eV}^{\infty} (\varepsilon - eV) \frac{F(\varepsilon)}{\sqrt{\varepsilon}}\, d\varepsilon \\ &= \frac{e S_p}{2\sqrt{2m}} \int_{eV}^{\infty} (\varepsilon - eV) f_p(\varepsilon)\, d\varepsilon. \end{aligned} \tag{8}$$

Here, S_p is the probe area. It is assumed that the probe is negatively biased ($V < 0$), and e is the electron charge (-1.6×10^{-19} C). The probe current is assumed to be directed to the probe. Double differentiation of equation (8) on the probe potential V gives the Druyvesteyn formula [4]:

$$\begin{aligned} \frac{d^2 I_e}{dV^2} &= \frac{2\pi e^3 S_p}{m^2} f_0(eV) = -\frac{e^2 S_p}{4}\sqrt{\frac{2e}{mV}} F(\varepsilon) \\ &= -\frac{e^2 S_p \varepsilon}{4}\sqrt{\frac{2e}{mV}} f_p(\varepsilon). \end{aligned} \tag{9}$$

Thus, measurements of I_e'' can provide

$$N = \frac{2\sqrt{2m}}{|e|S_p} \int_0^{-\infty} I_e''(V)\sqrt{V/e}\,dV \quad (10)$$

and

$$T_e = \frac{4\sqrt{2m}}{3NS_p} \int_0^{-\infty} I_e''(V)(V/e)^{3/2}\,dV. \quad (11)$$

There is another method of inferring EEDF directly from equation (8) by solving this integral equation using different regularization (deconvolution) procedures. The reader can find more on the subject in [21, 52]. To date, this method has not been routinely used in EEDF measurements due to its inferiority to EEDF measurement using the Druyvesteyn method.

2.3. What makes a good EEDF measurement?

EEDF measurements yield meaningful results only when they contain accurate information about the majority of electrons in both elastic ($\varepsilon < \varepsilon^*$) and inelastic ($\varepsilon > \varepsilon^*$) energy ranges, where ε^* is the excitation energy. The EEDF in the energy range between $\varepsilon = 0$ and $\varepsilon = T_e$ contains the majority of electrons and is responsible for evaluation of electron density and transport process. The distortion of this part of EEDF, which can be dramatic, significantly affects the accuracy of corresponding data found from the measured EEDF. The high-energy tail of the EEDF defines inelastic processes (such as excitation and ionization) and is very important for the kinetics of the excited and ionized states of atoms and molecules.

Acceptable EEPF data require that the energy gap between a zero point and the peak of the second derivative of the probe current not exceed $(0.3–0.5)T_e$, and that the high-energy tail beyond the inelastic threshold is not masked by noise and/or by ion current. This requirement calls for an EEPF-measurement instrument with a high dynamic range of approximately 60–80 dB and high-energy resolution of a fraction of T_e. Most of the published EEPF data obtained from laboratory experiments and commercial reactors (using homemade and commercial probe instruments) lack information about the bulk of low-energy electrons and the high-energy tail. The calculation of plasma parameters from these distorted EEPFs leads to errors and even the inability to analyse the EEPF tail responsible for excitation and ionization processes.

The simplicity of the concept upon which probe diagnostics are based has promoted the widespread illusion that the measurement, processing and interpretation of probe characteristics are commonplace and routine. Indeed, there is no plasma diagnostic method other than probe diagnostics where the danger of incorrect measurements and erroneous interpretation of the results is so great [8]. This statement, even in to a greater extent, is true in the measurement of EEDF due to the effects of error augmentation inherent to differentiation and regularization (deconvolution) procedures. In the measurement of probe I/V characteristics, it is important to realize that even small errors, which are tolerable in classic Langmuir-probe diagnostics, can result in enormous distortion in the inferred EEDF. Deterioration effects of probe contamination, circuit resistance and low-frequency and rf noise are practically invisible on the measured probe I/V characteristic but are usually clearly seen in the resultant EEDF. Therefore, to obtain a reliable EEPF, special attention must be paid to the accuracy of the probe measurements themselves and to the correct application and limitations of the traditional (Langmuir) probe method. Therefore, the next section is devoted to the consideration of the most common problems in probe measurements of EEDF and the methods of their mitigation.

3. Problems in probe measurements and their mitigation

3.1. Probe size

The inference of the EEDF from the measured volt/ampere characteristic of the probe immersed in plasma implies the validity of the very same assumptions as for the classical Langmuir-probe diagnostics. These assumptions require that the probe is small enough to avoid plasma and sheath perturbations beyond those accounted for in the probe theory [53, 54] (the application of probes for higher pressure and more exact evaluation of possible errors are discussed in section 4).

For a typical cylindrical probe, the following inequalities must be satisfied for the fulfilment of the small-probe assumption:

$$a \ln\left[\frac{\pi l}{4a}\right], b, \lambda_D \ll \lambda_e \qquad \text{and} \qquad I_p \ll I_d, I_r, I_z. \quad (12)$$

Here, a is the probe-tip radius, l is its length, b is the probe-holder radius, λ_D is the electron Debye radius, I_p is the probe current, I_d is the discharge current, I_r is the maximal current provided by the reference counter-electrode in the probe circuit (ion current to the grounded metal chamber, $I_r = I_B = S_{ch}eN_s\upsilon_B$, or electron-emission ability of the auxiliary cathode), and $I_z = e\Gamma_e$ is the current corresponding to the generation rate of electrons Γ_e with energy ε in the volume defined by the chamber characteristic size Λ or by the electron relaxation length λ_ε, whichever is shorter [19, 25, 55]. Here, S_{ch} is the chamber surface area, N_s is the plasma density near the chamber wall, υ_B is the ion sound (or Bohm) speed ($\upsilon_B = (T_e/M)^{1/2}$), M is the ion mass and I_B is Bohm current on counter-electrode. The value of Γ_e is sensitive to the electron energy but must be equal to I_B/e after being averaged over EEPF. For small discharge chambers, the flux of the fast electrons drawn to the probe may be comparable to their generation rate due to heating by the electromagnetic field and electron–electron collisions. In this case, the measured EEPF may be depleted with the high-energy electron tail. Note also that conditions (12) may be significantly more severe in electronegative gases [56]. In this case, negative ions can be repelled from the probe-holder at a distance significantly greater than λ_e, and the charged-particle density can be severely distorted near the probe surface, even if inequality (12) holds.

With increasing gas pressure and when the ratio of the plasma density at its boundary to that at the plasma centre, $N_s/N_0 \ll 1$, decreases, the wall-sheath resistance may not

be negligible compared with the probe-sheath resistance R_{psh} in the plasma centre. This situation leads to a redistribution of the voltage applied to the probe between the probe and the wall sheaths and results in a reduction of the electron current and a corresponding rounding of the measurement of the second derivative of the probe current in the vicinity of the plasma-space potential. The maximal sheath-resistance ratio at the chamber wall and the probe, $R_{csh}/R_{psh} = I_p/I_B$, occurs when the probe is at the plasma potential at which $R_{csh}/R_{psh} = (S_p N_0/S_{ch} N_s)(M/2\pi m)^{1/2}$, where $S_p = 2\pi al$. Thus, to neglect the voltage drop across the wall sheath, the following requirement must be satisfied:

$$(S_p N_0/S_{ch} N_s)(M/2\pi m)^{1/2} \ll 1. \qquad (13)$$

Note that inequality (13) is derived for Maxwellian EEPF. In argon (and in other Ramsauer gases), a CCP at low pressure has a bi-Maxwellian EEPF with a low-energy peak corresponding to the electron temperature T_{el} and a tail of hot electrons corresponding to electron temperatures T_{he}, where $T_{el} \ll T_{he}$. In this condition, the probe resistance at the plasma potential is defined by T_{el}, whereas the sheath resistance at the wall with the floating potential reference to plasma is defined by T_{eh}. Here, inequality (13) becomes even stronger; $(T_{el}/T_{he})^{1/2} < 1$ should be on the right-hand side instead of 1. The effects of a final probe circuit resistance associated with the violation of inequality (13) on the distortion of the measured EEPF and a remedy to relax inequality (13) will be discussed later in this review.

The first inequality in (12) means that there are no electron–atom collisions in the probe perturbation area including the probe sheath and presheath. Note that this inequality is applied not only to the probe tip that collects the probe current but also to an adjacent insulated probe holder. In many published works, the probe-holder diameter is excessively large, causing plasma perturbation near the collecting probe tip. This perturbation is similar to that occurring near the chamber wall (the probe holder is acting as an undesirable wall) and occurs due to the plasma sink to the probe holder.

Examples of a probe design with minimized plasma perturbation near the probe are depicted in figures 1 and 2, which show the telescopic probe structure with a thin probe holder used for EEDF measurements in symmetrical CCP with argon gas [55]. Here, the probe holder is made of a thin-wall quartz capillary with a diameter of $b = 0.33$ mm and a length of 2 cm that transits to a stronger structure with a larger diameter. The probe has a sleeve that prevents electrical contact between the probe and the sputtered conductive material on the probe-holder surface. This sleeve is a necessity when measuring in CCP due to considerable electrode sputtering by ions accelerated in the electrode rf sheath. The probe structure includes the measurement probe P_1 and a ring reference probe (RP) P_2 used for low-frequency and rf noise suppression in the probe-measurement circuit that will be discussed later.

The probe diameter $2a$ and length are 76 μm and 6 mm, respectively. The results of the EEDF measurements performed with this probe can be found in [51, 55, 57–59], and some will be shown later. The low-perturbation probe used for basic ICP studies [51] and that developed for probe diagnostics in plasma-chemical rf reactors [60] are shown in figures 3 and 4, respectively.

In the telescopic probe structure used for measurement in argon ICP [51] shown in figure 3, the probe holder near the probe is twice as thin as that used in CCP. Despite the small probe tip ($a = 38$ μm, $l = 6$ mm, chamber conductive

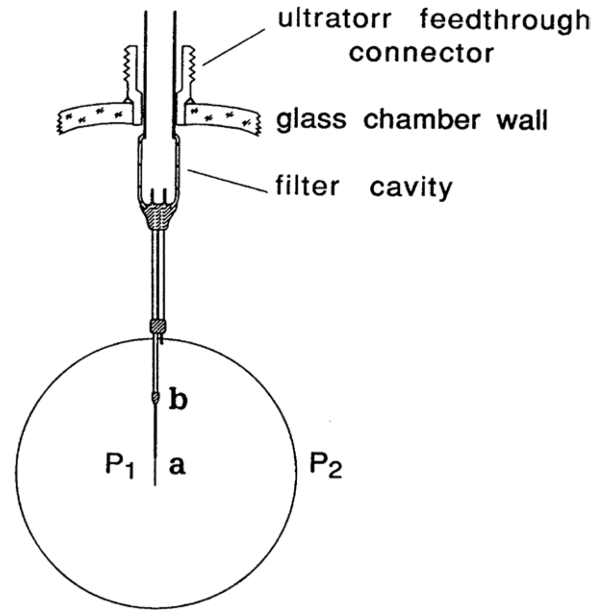

Figure 1. Telescopic probe P_1 with a ring reference probe P_2 used for EEDF measurement in CCP [55].

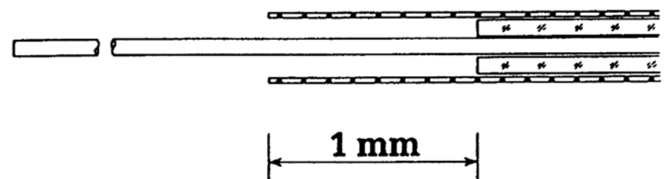

Figure 2. Probe with a thin-wall quartz protective sleeve used in the EEDF measurement in CCP [55].

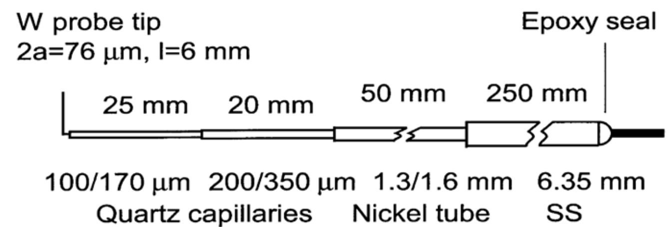

Figure 3. Telescopic probe used for EEDF measurement in argon ICP [55].

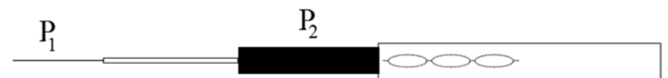

Figure 4. Low-perturbation rf-compensated probe for measurement in plasma reactors [60]. P_1 is the measuring probe with $a = 0.05$ mm. The probe holder has radius of $b = 0.5$ mm. P_2 is the reference probe for low-frequency noise suppression and acts as a shunting electrode for rf compensation.

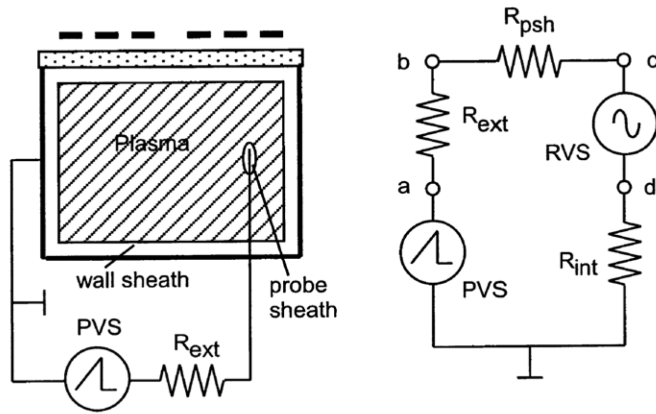

Figure 5. Probe-measuring configuration in plasma within a metal chamber (left) and its equivalent circuit (right) [51]. RVS is a residual voltage source, PVS is probe-voltage source, R_{psh} is probe-sheath resistance, R_{ext} is external resistance (includes all resistances between probe tip and voltage source) and R_{int} is internal resistance.

surface $S_{ch} \approx 0.1\,m^2$) and the electronics compensating the voltage drop across the chamber-wall sheath, the upper limit of argon pressure at which measurement of EEDF is possible is 300 mTorr. At higher gas pressure, the electron current to the probe that is limited by the ion saturation current to the chamber wall prevents the probe from reaching the plasma potential. The volt–ampere characteristic of the wall sheath is that of an ideal flat probe corresponding to near-infinite differential resistance in the area of the ion saturation current. For this reason, it is impossible to reach the plasma potential even after applying a very high voltage on the probe; the only result is an increase in the voltage across the chamber-wall sheath.

3.2. *Probe circuit resistance*

The resistance of the sheath at the chamber wall (or next to any other counter-electrode in the probe-current path) is only one of many causes of distortion in the measured probe characteristic and its second derivative. When making probe measurements, one usually assumes that the voltage applied to the probe is localized in the probe sheath around the probe tip. In reality, this voltage is distributed along different parts of the probe-current path. As a rule, the probe current and voltage measured directly at some point of the probe circuit are not the same as the current and voltage across the probe sheath.

The probe circuit configuration in application to an ICP with a grounded chamber and its equivalent circuit diagram are shown in figure 5. The probe current I_p flows from the grounded probe-voltage source (PVS) back to ground through various circuit elements along the current path: the external resistance R_{ext} (which includes all resistances located between the probe tip and the PVS), the probe-sheath resistance R_{psh} and the internal resistance R_{int} consisting of the chamber sheath resistance R_{csh}, the contaminated chamber surface resistance R_x and the probe presheath R_{pl} resistance, $R_{int} = R_{csh} + R_x + R_{pl}$. The plasma potential source, RVS (generally containing dc, low-frequency and rf components), is shown in the equivalent circuit as a residual (noise) voltage source. The external resistance is $R_{ext} = R_w + R_t + R_v + R_f$, where R_w is the resistance of the lead wires, R_t is the contact resistance, R_v is the sensor resistance and R_f is the rf-filter resistance at dc and low frequencies. Note that the rf-filter reactance $X_f = (L_f/I_p)\mathrm{d}I_p/\mathrm{d}t$ may also affect the probe circuit impedance at fast probe-voltage scans.

As a result of the aforementioned resistances, except for the probe-sheath resistance, the total probe circuit resistance $R_c = R_{ext} + R_{int} = R_w + R_t + R_v + R_f + R_{csh} + R_x + R_{pl}$. Some of these resistances (such as R_w, R_t, R_v and R_f) are constant during the probe scan and can be accounted for by processing the probe characteristic. Others (such as R_{csh} and R_x) are unknown, sometimes non-linear (thus, probe-current dependent) and generally not easy or even impossible to evaluate and account for. In practice, the probe voltage referenced to the ground, V_a, is measured at the far end of the probe lead wire, point 'a' in figure 5. Therefore, it includes not only the voltage drop across the probe sheath V but also the voltage drops across the external resistor $V_{ext} = I_p R_{ext}$, the voltage across the internal resistance $V_{int} = I_p R_{int}$ and the residual voltage V_r. Thus, the voltage applied to the probe is $V_a = V + V_{ext} + V_{int} + V_r$. To infer the true voltage across the probe sheath V, one has to account for stray voltages V_{ext}, V_{int} and V_r, which are not always negligible. On the other hand, the presheath plasma resistance R_{pl} is negligibly small in low-pressure gas-discharge plasmas, $R_{pl}/R_{po} \approx (a/\lambda_e)\ln(\frac{\pi l}{4a}) \ll 1$, where R_{po} is the minimal value of the probe-sheath resistance.

The probe circuit resistance significantly affects the probe I/V characteristic near the plasma potential where the probe current reaches its maximum and the probe-sheath resistance its minimum. For Maxwellian plasma, the minimal probe-sheath resistance $R_{po} = \mathrm{d}V/\mathrm{d}I_p|_{V=0} = T_e/eI_{po}$, where $I_{po} = I_p|_{V=0}$ is the electron saturation current. Due to error magnification inherent to the differentiation procedure, even a relatively small distortion in the I/V probe characteristic results in an enormous distortion in the inferred EEPF. This distortion manifests itself in the suppression and flattening of the second derivative of the probe I/V characteristic, $\mathrm{d}^2I_p/\mathrm{d}V^2$, near the plasma potential and an increased voltage interval between the second-derivative maximum and the zero-crossing point. The EEPF is proportional to $\mathrm{d}^2I_p/\mathrm{d}V^2$ and, when distorted in such manner, looks like a Druyvesteyn-like distribution (EEPF $\sim \exp(-\varepsilon^2/\langle\varepsilon\rangle^2)$). This 'Druyvesteynization' of an EEPF with increasing discharge power and/or gas pressure can be seen in the measurements of many authors and has even been mistaken for a new plasma kinetic effect in ICP.

EEPF depletion due to probe circuit resistance is proportional to $(\Delta V)^3$, where ΔV is the voltage drop across the circuit resistance and is most significant near the plasma potential, which corresponds to the low-energy electrons of the distribution. EEPF distortion depends on the ratio R_c/R_{po}, where R_{po} is the minimal probe differential resistance (at plasma potential) $R_{po} = T_e/eI_{eo}$ and I_{eo} is the electron saturation current. The distortion of $\mathrm{d}^2I_p/\mathrm{d}V^2$ for Maxwellian EEDF caused by final probe circuit resistance is demonstrated in figure 6. Here, the distorted shapes of $\mathrm{d}^2I_p/\mathrm{d}V^2$ that are

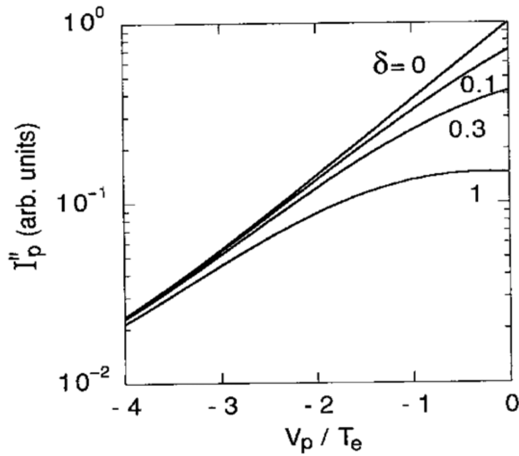

Figure 6. Second derivative (absolute value) of the probe electron current for Maxwellian EEDF for different parameters $\delta = R_{po}/R_c$. The Druyvesteynization effect is seen for large δ [55].

proportional to EEPFs are shown for the different parameters $\delta = R_c/R_{po}$. The EEPFs are dramatically distorted when the probe circuit resistance approaches the probe-sheath resistance. A calculation shows that the depletion of the second derivative of the probe current at the plasma potential due to probe circuit resistance by less than 3% requires the total probe circuit resistance R_c to be one hundred times smaller than R_{po}. This finding implies that, for undistorted EEDF measurements in high-density plasma, typical of ICP and Helicon plasma sources, R_c should be in the range of a few milliohms to tenths of an ohm. This requirement may not be easily achieved for a probe circuit having many resistive components, such as a filter choke and plasma to chamber-wall resistance.

This problem is severe in ICP with plasma-processing gases, where the metal chamber wall is covered with a low-conductivity layer of the plasma reaction products (large R_x). Even in argon ICP with clean chamber walls, the wall-sheath resistance R_{csh} is frequently comparable to the probe-sheath resistance near the plasma potential, resulting in the Druyvesteynization of the measured EEPF. The wall-sheath resistances, R_{csh} and R_x, also limit the maximum accessible gas pressure for ICP probe diagnostics when the ion current to the chamber wall is less than the electron saturation current to the probe, considered above.

The Druyvesteynization of EEPF and saturation of the plasma density with increasing gas pressure found in some published ICP probe measurements is generally the result of the finite probe circuit resistance. This effect is more pronounced at relatively high gas pressures when the plasma density near the chamber wall, N_s, is much smaller than that in the plasma bulk ($N_s \ll N_0$). Note that, in bounded diffusion-controlled plasmas, $N_s/N_0 \sim \lambda_i/\Lambda$ when $\lambda_i/\Lambda < T_g/T_e$ and $N_s/N_0 \sim (\lambda_i/\Lambda)^{1/2}$ when $\lambda_i/\Lambda > T_g/T_e$, where N_0 is the plasma density in the discharge centre, λ_i is the ion mean free path and T_g is the gas temperature [61].

The problem of the unaccounted resistance of the probe-current path remains unresolved in majority of ICP (and in other high-density plasma sources) probe experiments performed with homemade and commercial probe systems,

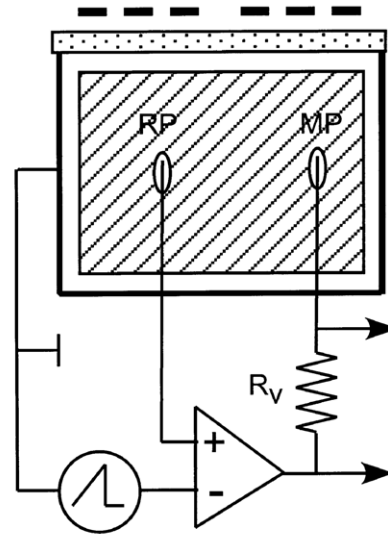

Figure 7. Probe driver circuit with a differential input for compensation of the dc plasma potential, low-frequency noise and internal resistance. The reference probe feeds into the positive input while the measuring probe voltage feeds into the negative input, providing the driver output with the difference between the ramp and plasma potential voltages [51] . MP is a measurement probe, RP is a reference probe and R_v is a sensor resistor.

resulting in a large EEPF distortion in its low-energy range. This distortion manifests itself as an enormous depletion (and even, absence) of low-energy electrons in the measured EEPF, whereas low-energy electrons constitute the overwhelming majority of the distribution. Consequently, using large Langmuir probes exacerbates the problems associated with the circuit resistance.

Different approaches (for different elements in the probe-current path) are employed in the probe experiment to address the issue of circuit resistance. The residual voltage V_r (that consists of dc, low frequency and rf voltages developed by RVS) and the voltage drop V_{int} across the internal resistance define the instantaneous value of the plasma potential reference to ground $V_{pl} = V_r + V_{int}$, can be cancelled by a probe-voltage driver having differential input, as shown in figure 7. The negative input of the driver is fed with the source of the PVS, whereas the RP signal corresponding to its floating potential (point c in figure 5) is fed to the positive input, thus producing a difference between these two input signals at the driver output. This difference cancels the dc voltage bias, low-frequency noise and the chamber-wall voltage drop. For effective noise cancellation the driver should have sufficient bandwidth in frequency and phase space. The dc bias and the chamber-wall voltage-drop compensation are limited by the maximum output voltage available from the driver. The probe driver shown in figure 7 does not compensate for time variation in the probe current due to plasma-density and electron-temperature (or EEDF) oscillations. Therefore, it can be used for the diagnostics of periodically varied plasmas in a time-resolved mode with appropriate signal-acquisition and processing probe waveforms [62]. On the other hand, this measurement technique has limitations when working with strongly unstable plasma. It is impractical to use the RP feedback for the purpose of rf-noise suppression associated

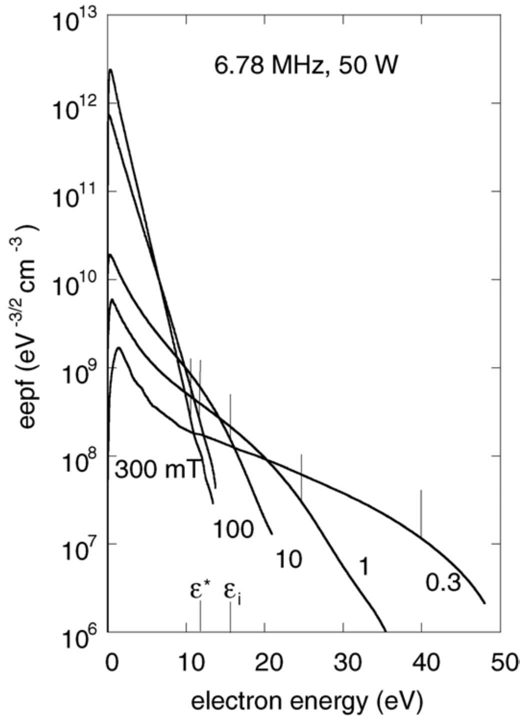

Figure 8. EEPFs measured in argon ICP between 0.3 and 300 mTorr. ε^* and ε_i denote the excitation and ionization energies, respectively. Vertical lines show the dc plasma potentials referenced to a grounded chamber [51].

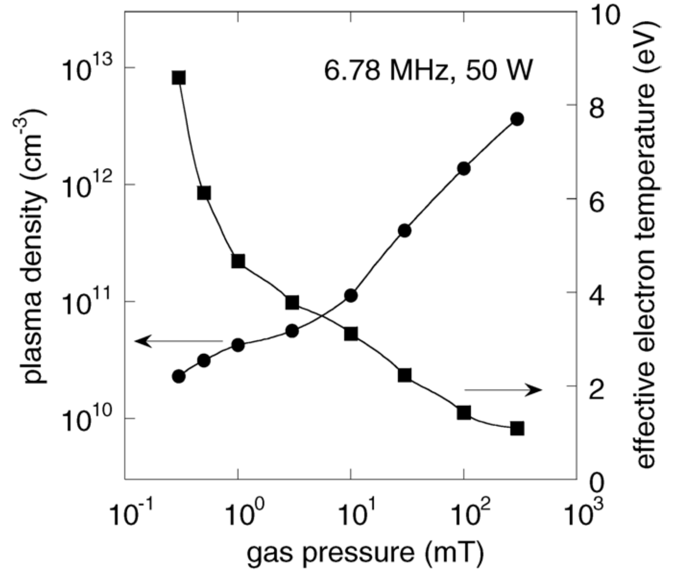

Figure 9. Plasma density and effective electron temperature $T_e = 2/3\langle\varepsilon\rangle$ found as the corresponding integrals of the measured EEPFs shown in figure 8.

with the discharge driving frequency and its harmonics due to the speed limitation of the available electronics. Approaches to mitigating the effects of internal resistance and low-frequency noise, considered above, have been implemented in past EEDF measurements in CCP [55], in ICP [51] and in commercial instrument VGPS of Plasma Sensors® [60].

EEPFs measured in argon ICP driven at 6.78 MHz at discharge power of 50 W are shown in figure 8 for wide range of gas pressures [51]. The measurements were performed with the probe shown in figure 3 and with compensated internal probe circuit resistance, in a Faraday-shielded ICP with negligibly low rf plasma potential and no need for probe rf compensation. The basic plasma parameters obtained from the measured EEPFs, N and T_e, are shown in figure 9.

Note the presence of a well reproduced Maxwellian distribution in the low-energy part of the EEPFs at relatively high argon pressure, where the plasma density is sufficiently large to provide a strong Maxwellizing effect due to electron–electron (e–e) collisions. The frequency of e–e collisions ν_{ee} is proportional to $N\varepsilon^{-3/2}$; therefore, for electron energies of less than average one $\langle\varepsilon\rangle$ and for $N(\langle\varepsilon\rangle/e)^{-3/2}$ larger than approximately 10^{10} (cm V^2)$^{-3}$, the EEPF must be Maxwellian. The larger the plasma density, the larger is the energy range where the EEPF coincides with a Maxwellian distribution.

Figure 10(a) shows another example of EEPFs measured in an industrial ICP reactor with the VGPS of Plasma Sensors® probe instrument [63] with an rf-compensated probe, shown in figure 3, and compensated R_{int}. For comparison, the result of the measurement made in the same plasma with the Espion of Hiden® probe system is shown in figure 10(b). A dramatic

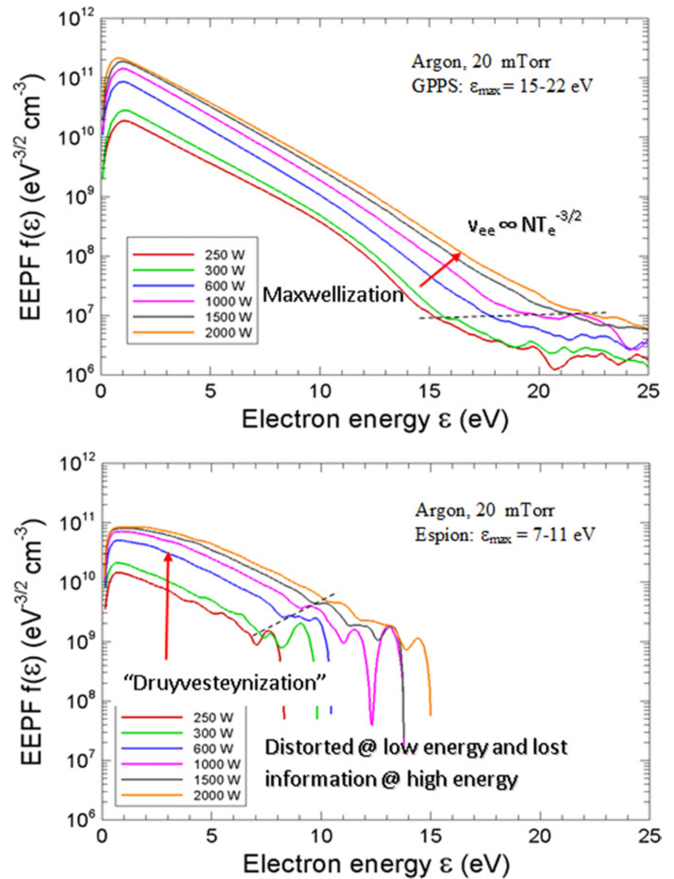

Figure 10. EEPFs measured with different probe systems in an industrial ICP etcher for a range of discharge powers between 0.25 and 2 kW. The dashed lines show the noise threshold that defines the maximal resolved electron energy ε_{max}. Note a Maxwellization effect with increasing rf power at high electron energies (in figure 10(a)), in contrast to the Druyvesteynization effect at low electron energies (in figure 10(b)).

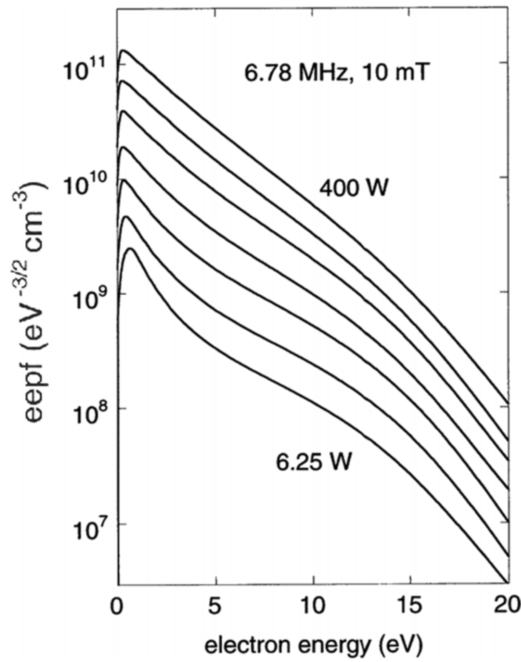

Figure 11. EEPFs measured in argon ICP in a wide range of discharge powers [44]. The EEPFs are shown in doubling power increments. Note the EEPF Maxwellization in the elastic energy range ($\varepsilon < \varepsilon^*$) with increasing rf power [51].

distortion in the low-energy portion of the EEPF, showing a Druyvesteyn-like distribution in figure 10(*b*), is apparent. The difference between the measurements in figures 10(*a*) and (*b*) and the divergence between the measured and Maxwellian distribution in figure 10(*b*) increase with rf power and, thus, with plasma density. The finding in figure 10(*b*) is obviously opposite to the well-known trend of EEDF behaviour in gas-discharge plasmas. The Maxwellizing effect, increasing with plasma density, is clearly seen in the EEPF measured in a wide range of discharge powers in argon ICP presented in figure 11 [51].

The RP does not compensate for the voltage drop in external resistance R_{ext}. Fortunately, however, this external resistance can be readily measured and accounted for in probe characteristic processing. It can also be accomplished with an analogue circuit known as a gyrator, which is a current-to-voltage converter with a negative input resistance equal to R_{ext} [55].

3.3. Plasma oscillation

Probe characteristic distortion in rf plasma is a well-recognized problem and has been analysed in many works [19, 21, 55, 64–69]. Nonetheless, this issue has not been properly addressed in many published experiments performed with rf plasmas. Some authors believe that simply putting some filter tuned on the discharge driving frequency and its harmonics into the probe circuit is sufficient to address the probe distortion associated with rf oscillation. Indeed, it has been shown experimentally [65] that, to avoid a noticeable distortion in EEDF measurement, the rms rf voltage in the probe sheath, V_{shrf}, should be two to three times less than the electron temperature expressed in volts, $V_{\text{shrf}} < (0.3\text{–}0.5)T_{\text{e}}/e$. To fulfil this requirement, the probe filter system must satisfy to the following relationship between the filter and probe parameters:

$$|Z_{\text{pr}}/Z_{\text{f}}| \leqslant (0.3-0.5)T_{\text{e}}/|eV_{\text{prf}}|. \qquad (14)$$

Here, Z_{pr} is the impedance between the probe and plasma, Z_{f} is the filter impedance, V_{prf} is the rms rf plasma potential referenced to ground.

There are several ways to minimize V_{shrf}. One is to design a rf plasma system with a reduced or even negligibly small rf plasma potential V_{prf}. Examples of this approach have been demonstrated in [51, 68] and partially in [55]. The second and most common approach is the use of rf filters mentioned above [19, 55, 66, 69]. Another method is the biasing of the measuring probe with rf voltages (of fundamental frequency and few upper harmonics) with amplitudes and phases equal to those of the plasma rf potential [70, 71]. This approach is preferable for measurements in rf plasma with a large rf-electric-field gradient, such as near the electrode area of a CCP and the skin layer of an ICP, where a large reference shunting electrode could introduce a considerable disturbance to the narrow localized rf field.

Now, let us consider the method of the realization of inequality (14) for a passive filter design. Relation (14) is practically impossible to satisfy when Z_{pr} is defined solely by the probe-sheath impedance, usually corresponding to a reactance of the probe-sheath capacitance of less than 1 pF. Therefore, a shunting electrode is placed in the probe vicinity or in the area that is rf equipotential with the rf plasma potential near the measuring probe [19, 21, 55, 69]. The shunting electrode is connected to the probe with a capacitor whose capacitance is much larger than the probe-sheath capacitance but is small enough not to introduce a noticeable stray displacement current into the probe-measurement circuit. With the shunting electrode, the impedance of the probe referenced to plasma can be reduced by one to two orders of magnitude.

According to (14), the required filter impedance is defined by the value of V_{prf} for each harmonic of the plasma potential spectrum to be measured. Unfortunately, the straightforward way of measuring of V_{prf} (by connecting a scope rf probe to the measuring Langmuir probe) usually results in a value that is an order of magnitude lower than the true rf plasma potential. The reason for this error is that the input capacitance of a rf probe C_{in} is much larger than the capacitance of the Langmuir probe referenced to plasma C_{pr}, whereas the reverse relationship is a must for the correct measurement of V_{prf}. With typical $C_{\text{pr}} \approx 1$ pF and $C_{\text{in}} \approx 15$ pF (for a 1 : 10 rf probe), V_{prf} measured this way is approximately 16 times less than its true value.

The authors recommend the following procedure to measure the true rf plasma potential (see also [72]). Temporarily insert into the plasma a relatively large probe (electrode), perhaps 3–6 mm OD, and a 5–10 cm long metal road (tube) connected via a 1 : 100 rf voltage probe-divider (usually having $C_{\text{in}} = 3\text{–}5$ pF) to the high-impedance input of a spectrum analyser. Depending on the electrode size and plasma density, its capacitance C_{pr} will be on the order of

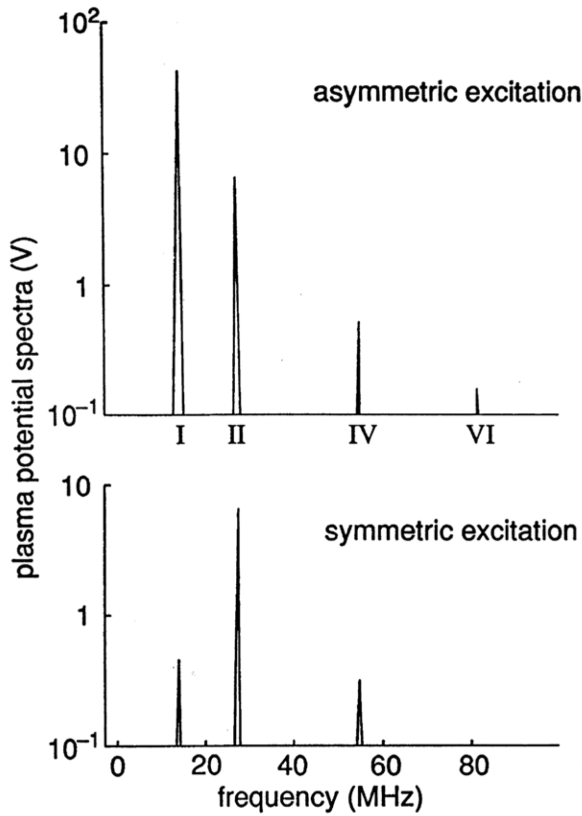

Figure 12. Plasma potential spectrum measured in argon CCP driven at 13.56 MHz [55].

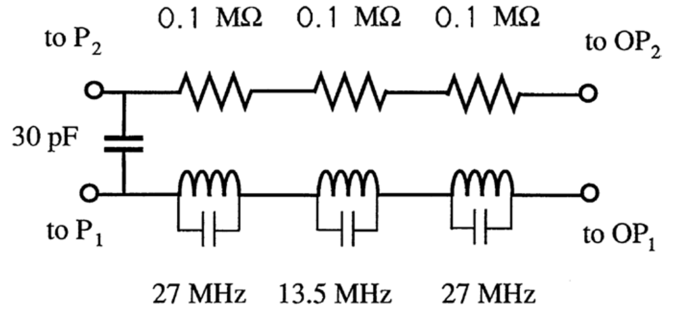

Figure 13. Two-channel (for the measuring and the reference probes) rf filter built according to the data shown in figure 12 [55].

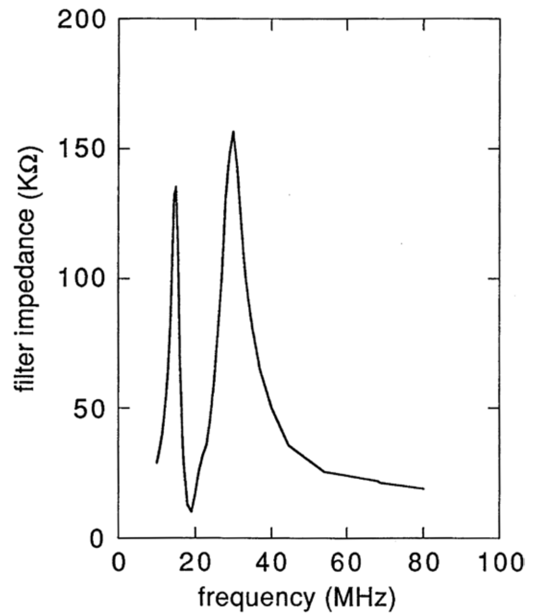

Figure 14. Filter impedance versus frequency of the two-channel filter shown in figure 13 [55].

100 pF, providing 5% accuracy in the measurement of V_{prf} (for each harmonic) with a voltage divider having $C_{in} = 5$ pF.

The probe–plasma coupling impedance at the probe floating dc potential is practically defined by the shunting electrode impedance $|Z_{pr}| = [(\omega C_{pr})^2 + (eI_B/T_e)^2]^{-1/2}$ and can be readily evaluated for a known electrode surface and expected plasma parameters N and T_e (see, e.g., [25]). The second term in the expression for Z_{pr} is due to the electrode-sheath conductivity and dominates at frequencies lower than the ion-plasma frequency, $\omega < \omega_i$. With values of Z_{pr} and V_{prf}, one can determine the required minimal filter impedance for each harmonic of V_{prf} whose rms value is larger than $(0.3–0.5)T_e/e$

$$Z_f \geqslant (2-3)Z_{pr}|eV_{prf}|/T_e. \tag{15}$$

To maximize the filter impedance, parallel resonance tanks tuned to each relevant harmonic are used: $Z_f = Q\omega L = Q(\omega C)^{-1}$. Here, L is the inductance, C is the filter capacitance and Q is its Q-factor. Subminiature inductive chokes with self-resonance frequencies matching the plasma potential spectrum are the most suitable for filter construction. Their winding stray capacitance C_0 is around 1 pF, and Q is around 10. Having a minimal possible resonating capacitance and a relatively large bandwidth $\Delta\omega = \omega/Q$, they provide high filter impedance even considering some detuning caused by the filter enclosure and plasma proximity.

Examples of the successful implementation of the above-considered procedures and recommendations are presented in figures 12–16. The plasma rf potential spectra measured in the mid-plane of an argon CCP driven at 13.56 MHz are shown in figure 12. As seen in figure 12, the symmetrical drive of CCP ensures a significant reduction in the fundamental (and supposedly all odd) harmonic of the plasma rf potential that essentially relaxes the requirements for rf-filter complexity.

A two-channel rf-filter circuit designed for this CCP and its impedance are shown, respectively, in figures 13 and 14. The measuring probe branch of the filter consists of sub-miniature (6 mm long, 1.8 mm diameter) chokes self-resonating at 13.6 and 27.2 MHz. The RP branch of the filter consists of three resistors (to reduce their total capacitance). The high resistance of this branch is of no concern to sense the dc and low-frequency components of the plasma potential because it is a part of the 10 MΩ voltage divider on the input of the probe driver shown in figure 15. The filter is connected to the measuring probe P_1 and the ring RP P_2 that is simultaneously acting as a rf shunting electrode connected to the measuring probe via a small capacitor. The use of a ring RP provides a sufficiently large surface (for shunting) and minimal plasma global and local (close to P_1) disturbance.

The complete probe-measurement diagram is shown in figure 15. The plasma potential, passing rf filter F and a

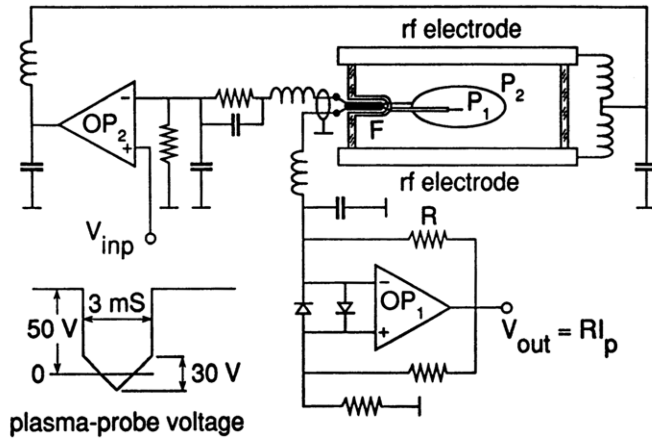

Figure 15. Circuit diagram for EEPF measurement in a symmetrically driven CCP [55]. The circuit incorporates compensation for the dc voltage in the electrode rf sheath, low-frequency noise, rf plasma potential and the external dc resistance of the rf filter shown in figure 13. The filter (external) dc resistance is compensated by a current-to-voltage converter (OP_1) with negative input resistance. Input wave form being amplified by 10 times have opposite polarity than probe voltage.

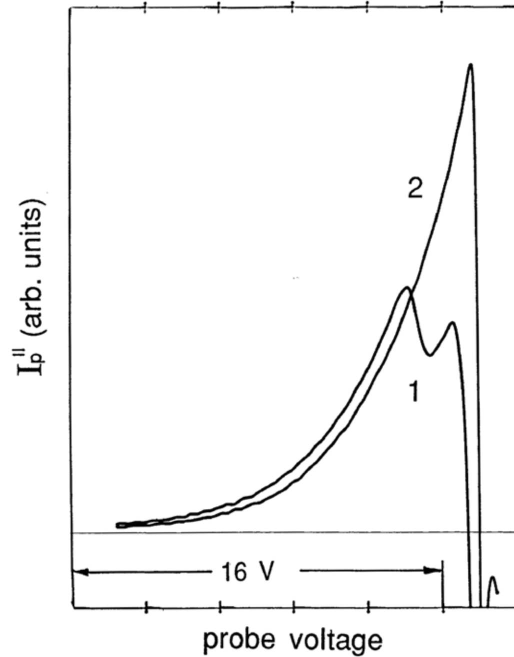

Figure 16. Second derivative of the probe characteristic (proportional to EEPF) measured in helium CCP at 13.56 MHz without the filter, curve 1, and with the filter, curve 2 [55] . Note the distance between the maximum and zero-crossing points of undisturbed I_p'', $\Delta V \ll T_e \approx 5$ eV.

voltage divider (10 : 1), is fed to the input of the probe driver OP_2 with a gain of $G = 10$. The probe span voltage is applied to the rf electrodes of CCP, whereas the measuring probe P_1 is ground via a current-to-voltage converter OP_1 having a negative input resistance equal to the dc resistance of the rf filter (27 Ω). The parameters of the probe ramp voltage are shown in figure 15. To maintain a clean probe surface, the probe is biased with a high negative voltage (−50 V referenced to its floating potential) between the probe-voltage ramps. The effect of the rf-noise suppression with the arrangement described above in a helium CCP symmetrically driven at 13.56 MHz is shown in figure 16.

Examples of the EEPF measurements in a CCP are given in figures 17–20. In figure 17, the measured EEPFs in an argon CCP driven at 13.56 MHz and 30 mTorr are shown as functions of the electron total energy (kinetic plus potential) at different axial positions along the rf electric field [73]. Under this condition of a strong electron kinetic non-locality [74–76], the EEPFs measured at different positions of a non-uniform plasma coincide. The EEPFs measured in the same CCP running at 300 mTorr and shown in figure 18 demonstrate mixed behaviour: nonlocal in the elastic energy range of $\varepsilon < \varepsilon^*$ and local-like in the inelastic energy range of $\varepsilon > \varepsilon^*$. Another example of EEPF measurement demonstrating a CCP transition in helium gas from the α mode to the γ mode [58, 77] is shown in figure 19. The change in the electron temperature and the plasma density corresponding to the measured EEPF during the mode transition is shown in figure 20.

A special situation arises in rf plasmas with a large rf-field gradient, such as in the near rf electrode area of a CCP and in the skin layer of an ICP. In the last case, the situation can be exacerbated in low-frequency ICPs operating in the non-linear regime when a significant rf polarization field of the second harmonic (much larger than the induction-heating rf field for the fundamental harmonic) is induced normal

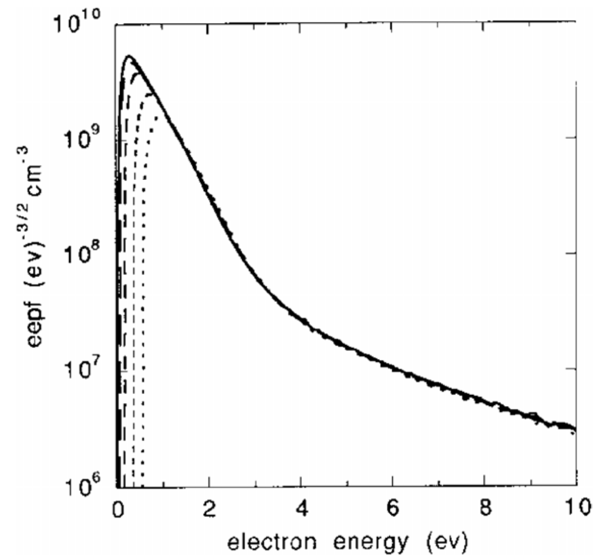

Figure 17. EEPFs measured at different axial positions in argon CCP at 30 mTorr [73] . The solid curve corresponds to the CCP mid-plane, whereas the dotted curve corresponds to a position close to the plasma boundary.

to the skin layer due to the interaction of the rf magnetic field with the rf current [78, 79]. Significant gradients of the rf electric field arise in rf plasmas immersed in the dc magnetic field, when the rf discharge current induces a rf hole effect across the plasma [80]. Due to non-uniformity in the discharge rf current (and, sometimes, in the magnetic field), it is difficult to find a sufficiently large rf equipotential area to place the shunting probe in the vicinity of the measuring

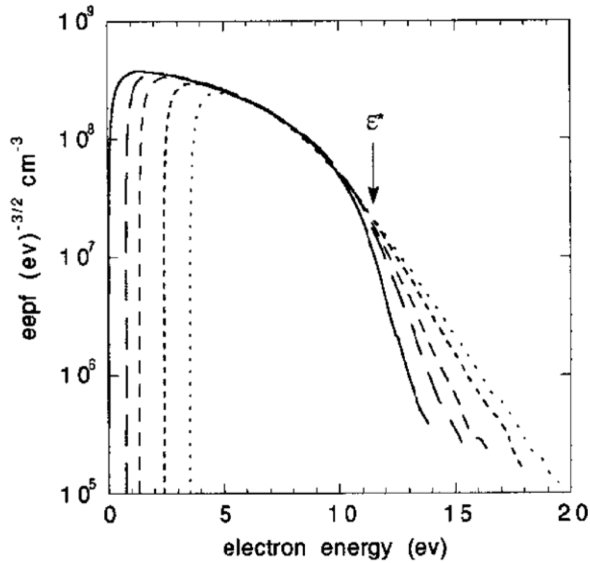

Figure 18. EEPFs measured at different axial positions in argon CCP at 300 mTorr [62]. The solid curve corresponds to the CCP mid-plane, whereas the dotted curve corresponds to a position close to the plasma boundary. ε^* denotes the excitation energy.

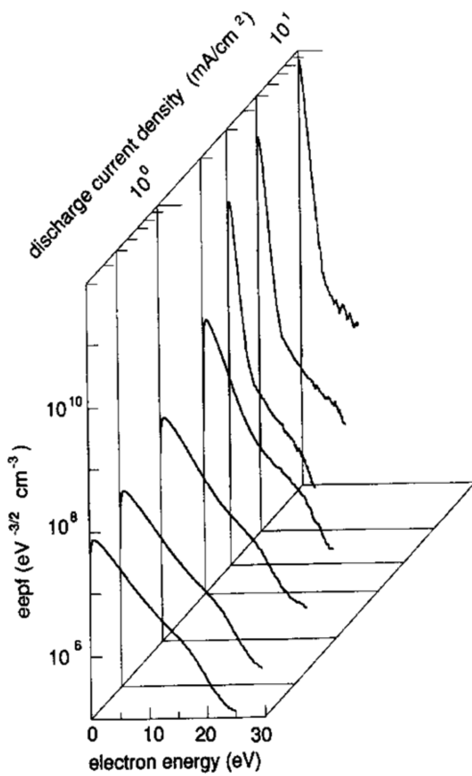

Figure 19. EEPF evolution during the transition of the helium CCP into the γ mode [58].

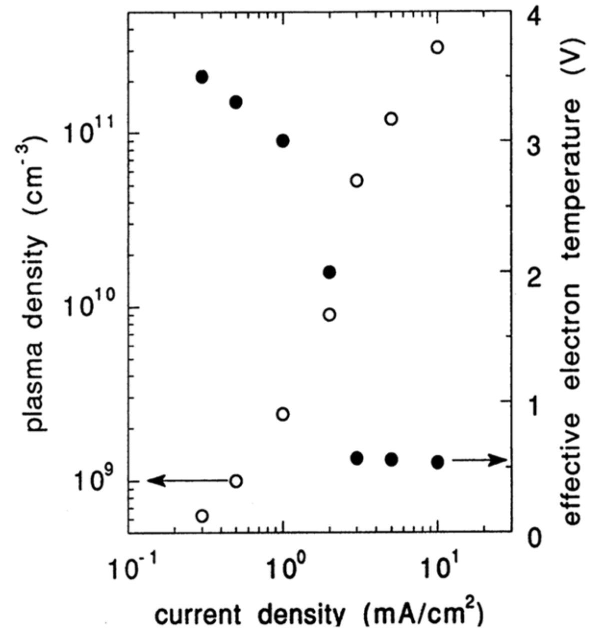

Figure 20. Plasma and discharge parameter evolution during the CCP transition to the γ mode [58].

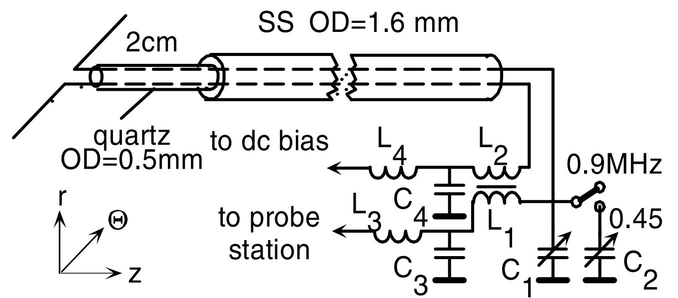

Figure 21. Probe circuit diagram for EEDF measurement in strongly non-uniform induction and polarization electric fields in ICP operating in the non-linear regime [81].

probe. In this case, the biasing of the measuring probe with a rf voltage equal to the plasma rf potential may be the only remedy to avoid rf distortions in the EEDF measurement. This method of mitigating the rf voltage in the probe sheath requires sophisticated analogue and digital electronics able to test numerous combinations of phases and amplitudes for each discharge condition.

A more simple, convenient and robust way is to bias the measuring probe with the plasma rf potential sampled with a dc-biased small RP placed close to the measuring probe. The circuit diagram of an arrangement used for EEPF measurement in the skin layer of a low-frequency (0.45 MHz) pancake ICP operating in the non-linear regime is shown in figure 21 [81]. To increase the coupling between the plasma and the RP (figure 21, top), the probe is biased to be near the plasma potential, where the probe sheath has a minimal resistance. A source of dc current (with high output resistance) must be used to prevent the shunting of the RP by the dc current source. The primary winding (L_2) of the 1 : 1 transformer connected between the RP and the biasing source induces the rf plasma potential that rf biases the measuring probe on the secondary winding (L_1). The transformer with bifilarly wound, L_1 and L_2, is resonated at 0.9 MHz with trimmer capacitor C_1 connected to L_1, resulting in an increase in its impedance in $Q \approx 60$ times, thereby acting as a high-impedance rf filter. Both probes were azimuthally oriented along the induction rf field, and the EEPF measurements were performed along the axial direction.

3.4. Time-resolved EEDF

Time-resolved EEDF-measurement techniques have been considered in reviews [19, 21] and in works cited therein. Since then, considerable improvement in the probe data acquisition and digital-processing technique has been achieved. There are two approaches to the measurement of EEDF in time-variable plasmas. One is the instant measurement of the probe characteristic during a probe scan time τ_s much shorter than the plasma transient process τ_p, when the EEDF change during the measurement is negligible. This method has speed limitations associated with transient processes in the probe sheath and surrounding plasma (presheath) and with probe-sheath capacitance and probe stray capacitance to the plasma and to the ground.

At low gas pressure defined by the condition (12), the electron transient time τ_e across the probe sheath is on the order of ω_e^{-1}, where ω_e is the electron-plasma frequency. Thus, τ_e is negligibly small compared with the usual plasma transient time τ_p. The ion transient time τ_i, which is on the order of ω_i^{-1}, where ω_i is the ion-plasma frequency, is irrelevant to EEDF measurement because usually $d^2I_i/dV^2 \ll d^2I_e/dV^2$. The real limiting factor affecting speed of the probe measurement is the displacement currents I_c due to probe-sheath capacitance (probe tip, and probe holder) to plasma and due to probe lead capacitance to ground.

The sheath capacitance is non-linear and frequency dependent and is thus dependent on both V and dV/dt [82, 83]. For a small, time-variable amplitude of the sheath voltage V_t ($V = V_{dc} + V_t$ and $V_t \ll V_{dc}$), the displacement current across the sheath at the floating potential ($V_{dc} = V_{fl} \approx (3\text{–}5)T_e/e$) is equal to the electron current ($I_c = I_e$) at $\omega = (3-5)\omega_i$. At more negative probe voltages and/or higher frequencies, $I_c > I_e$ and the contribution of d^2I_c/dV^2 may be comparable to d^2I_e/dV^2, resulting in EEDF distortion in the inelastic energy range ($\varepsilon > eV_{fl}, \varepsilon^*$). A rough criterion for a fast EEDF measurement unaffected by displacement current can be written as $V^{-1}dV/dt \ll \omega_i$, corresponding to maximal EEDF time resolution $\Delta t = (10\text{–}30)\omega_i^{-1}$. This value for Δt is usually much less than the characteristic time of the plasma parameter transient processes. For example, in the afterglow stage of a pulsed discharge, the plasma density decay time, $\tau_{pN} = N^{-1}dN/dt$ is $\tau_{pN} \approx \Lambda/v_B$, $\tau_{pN} \approx \Lambda^2/\lambda_i v_B$ and $\tau_{pN} \approx \Lambda^2/D_a$ for ion inertia, variable ion mobility and diffusion-controlled plasmas, respectively. Here, Λ is the plasma characteristic size, v_B is the ion sound speed, λ_i is the ion mean free path and D_a is the ambipolar diffusion coefficient. Note that the values of v_B and D_a in expressions for τ_{pN} are mainly defined by the cooled electron temperature at the late stage of afterglow. The electron temperature relaxation time $\tau_{pT} = T_e^{-1}dT_e/dt$ is always much smaller than τ_{pN} and, for low-pressure discharges, is defined by electron inelastic collisions (in the early afterglow stage) and by the escape of electrons to the chamber wall.

Given the non-linear and time-dependent nature of the sheath capacitance, it seems that there is no chance for an accurate accounting of the displacement current in the EEDF measurement. However, the maximal slue rate of the probe voltage, dV/dt, ensuring no EEDF distortion due to probe displacement current, can be found experimentally with a steady-state plasma and variable dV/dt.

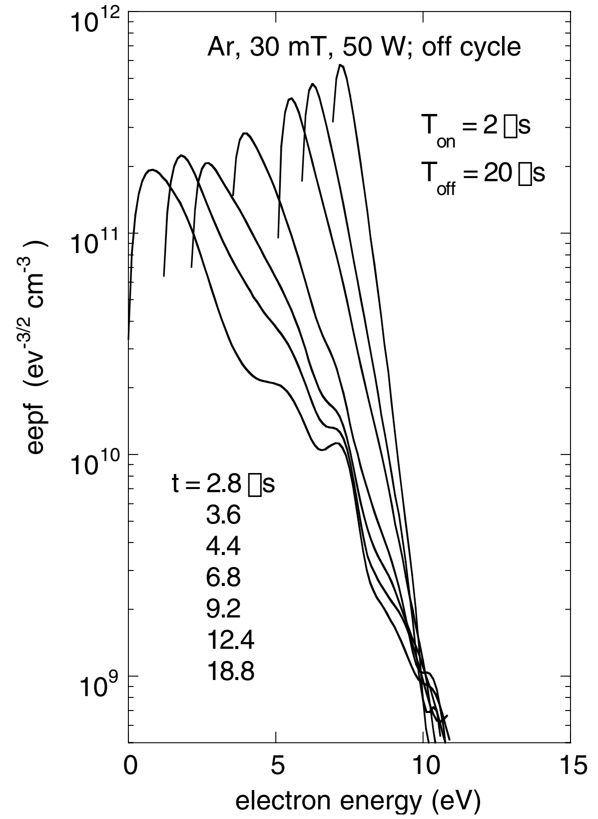

Figure 22. EEPF evolution in the afterglow stage of a periodically pulsed ICP [62]. The position of EEPF from left to right corresponds afterglow elapse time.

A more productive and successful method of time-resolved EEDF measurement (but only applicable to a time-periodic plasma, such as a repeatable pulse or low-frequency discharges) is the collection of many relatively slow probe scan data with the following rearrangement of the data points corresponding to the same phase of the transient process. With the speed and precision (1–10 MHz and 10–16 bit) of the modern digitizers of digital scopes and processing cards, the collection of 10^6–10^7 sample points is quite sufficient to obtain 10^3–10^4 data points averaged over 10^3 probe characteristic traces. With the probe scan time of 1 ms, 1000 sample points along each trace and averaging over 1000 traces, the measurement of EEDF in a large dynamic range (up to 60 dB) is possible with a resolution on the order of 1 μs.

Time-resolved EEDF measurements according to the above-described procedure have been recently performed in different kinds of ICP in pulsed and CW modes [62, 84–86]. The EEPF evolution in the afterglow stage of a periodically pulsed ICP ($T = 22\,\mu$s with duty factor 9%) is presented in figure 22 [62]. Here, seven EEPFs are shown in order from left to right according to the elapsed time t after the pulse end, starting at $t = 2.8\,\mu$s. The shift in the EEPF position along the energy axis corresponds to the plasma potential shift referenced to the plasma potential at $t = 2.8\,\mu$s. The origin of the EEPF irregularity at $t = 2.8\,\mu$s (rounding at small energy and oscillation at higher energy) is not clear. It may

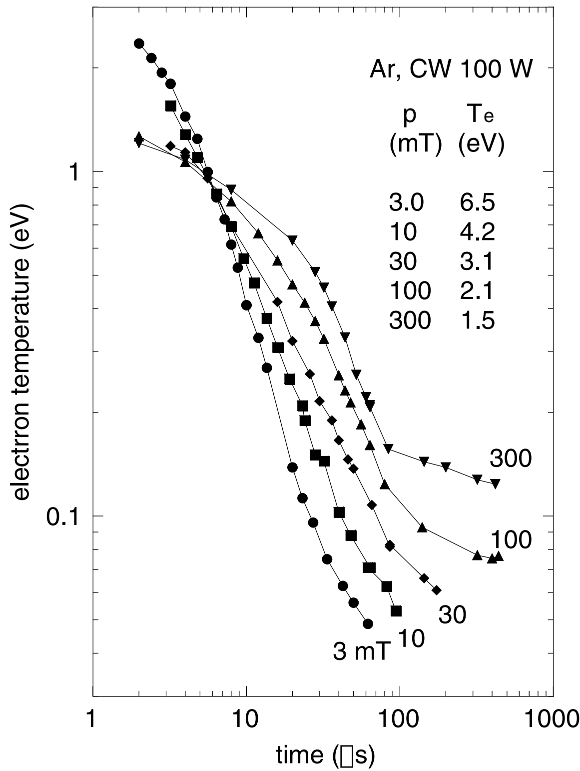

Figure 23. Evolution of electron temperature in the afterglow stage in a periodically pulsed ICP for different argon pressures [62].

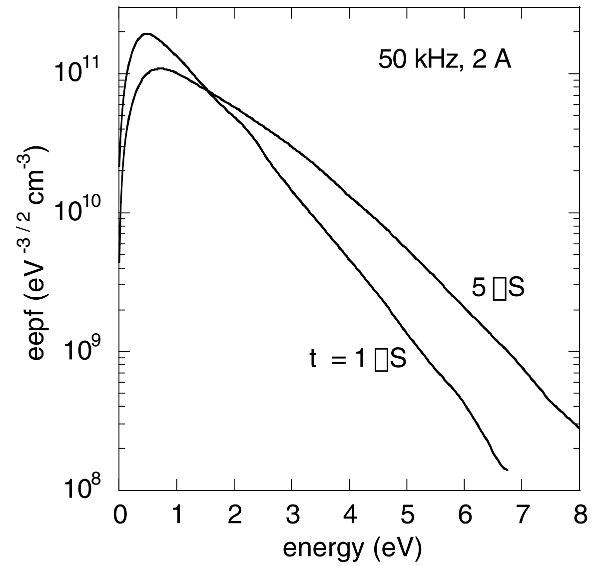

Figure 24. EEPFs measured in inductive hf light source at minimal ($t = 1\,\mu$s) and maximal ($t = 5\,\mu$s) instant electron temperature [86].

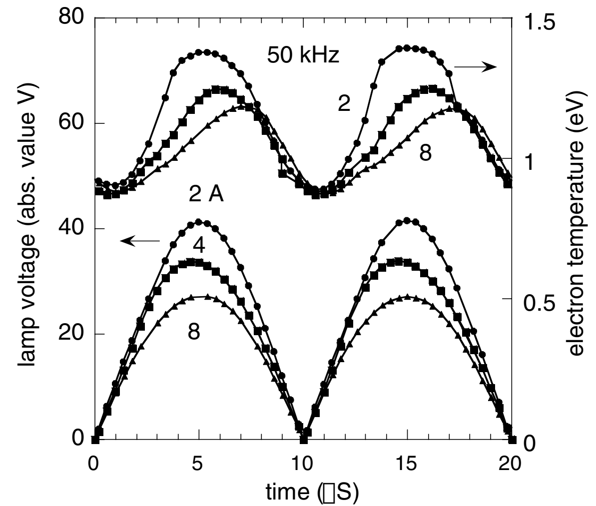

Figure 25. Electron-temperature and lamp-voltage variations during the rf period [86].

be associated with the plasma and/or the ringing effect of the measuring electronics immediately following the pulse.

The time evolution of the effective electron temperature $T_e = \frac{2}{3}\langle\varepsilon\rangle$ in the afterglow stage, found by the integration of the measured EEPFs in a periodically pulsed plasma ($T = 2$ ms with duty factor 50%) for different argon gas pressures, is shown in figure 23 [62]. The steady-state values of the electron temperature for different argon pressures are also shown. The electron cooling occurs more rapidly at lower gas pressures. The main mechanism of the electron cooling is the escape of electrons to the chamber wall (diffusion cooling) [62, 84, 87]. At 3 mTorr, 60 μs after the pulse, the electron temperature drops 130-fold from 6.5 eV in the steady state to 0.05 eV, which is close to room temperature.

EEPFs in a high-frequency (hf) inductive lamp filled with 0.3 Torr of argon and 7 mTorr of mercury and operating at 25–250 kHz were measured with 0.5 μs temporal resolution at different phases of the hf cycle in [86]. Two EEPFs corresponding to minimal ($t = 1\,\mu$s) and to maximal ($t = 5\,\mu$s) electron temperatures are shown in figure 24 for the lamp driven at 50 kHz with a 2 A discharge current. In these conditions, plasma density is essentially time independent because the hf period is much less than the plasma diffusion time $\tau_{pN} \approx \Lambda^2/D_a$. Calculated by the integration of the measured EEPF, the electron temperature along the hf period and the lamp voltage along the 60 cm closed discharge path are shown in figure 25. Note an asymmetry in the $T_e(t)$ wave form, the shift between the electron-temperature extremes and the corresponding discharge voltage extremes.

3.5. Ion-current effect

In measurements of EEPF proportional to the second derivative of the electron current to the probe $I_e'' \equiv d^2I_e/dV^2$, a differentiation procedure is usually applied to the whole probe current that consists of the electron and ion components. Therefore, one may expect an influence of the second derivative on the ion current $I_i'' \equiv d^2I_i/dV^2$ on the measured EEPF. This question was considered in [88, 89], where the ratio of I_e''/I_i'' as a function of the normalized probe voltage $\eta = -V/T_e$ was calculated for radial and orbital collisionless ion motion around a cylindrical probe for different shapes of EEPF and different values of a/λ_D. It has been shown that an appreciable influence of I_i'' may occur for thin probes, light gases and large negative probe voltages when the orbital-motion model is applicable for the ion current to the probe ($a/\lambda_D < 1$). Under this condition, when the effect of I_i'' is maximal, the expression for the ratio

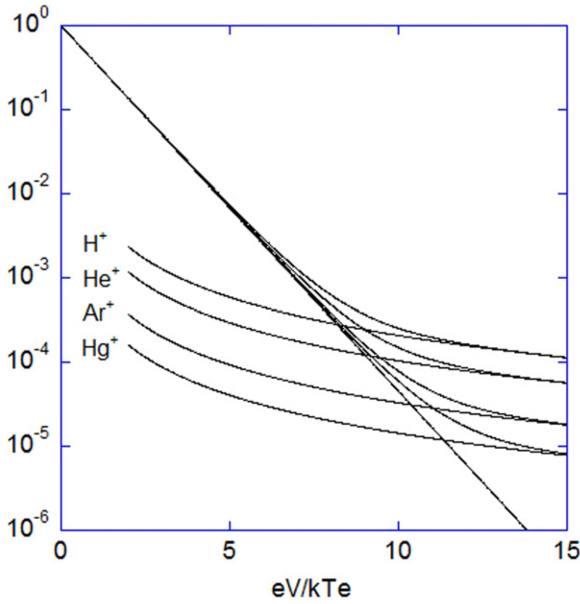

Figure 26. Normalized values of I_e'', I_i'' and I_p'' (absolute values) according to expression (16).

I_e''/I_i'' for a Maxwellian EEDF and $a/\lambda_D \ll 1$ was derived as

$$I_e''/I_i'' = (4\pi M/m)^{1/2}\eta^{3/2}\exp(-\eta). \qquad (16)$$

The ratio I_e''/I_i'' given by (16) does not depend on a/λ_D and can be used as an estimate for the maximal possible I_i'' effect in the assumption of a Maxwellian EEDF. Normalized values of I_e'', I_e'' and $I_p'' = I_e'' + I_i''$ are shown in figure 26 for different gases. Assuming the error due to I_i'' contribution to be within 10%, one can obtain the dynamic range of EEPF measurement unaffected by I_i'' in argon plasma as 66 dB (over three orders of magnitude) from (16) and figure 26. This dynamic range of EEPF measurements, corresponding to an energy span of $7.5T_e$, exceeds the dynamic range of the majority EEPF measurements in argon plasmas. In EEPF experiments, the dynamic range of EEPF measurements is limited by the low-frequency noise (sometimes mistakenly interpreted as a type of resonance effect in electron kinetics). The effect of I_i'' on EEPF measurement is usually considerably smaller than that given by (16), except for very thin probes, low-density plasmas and some special EEPF shapes. The effect of I_i'' on EEPF manifests itself as a slowdown in the drop of the function $\ln[I_p''(V)]$, at large negative probe voltages seen in figures 26 and 27.

Both electron and ion currents to the probe (and their derivatives) essentially depend on the shape of EEPF [90]. The authors of [89] calculated and compared the values of I_e'' and I_i'' for non-Maxwellian EEPFs for orbital and radial ion motion. They considered a class of EEPFs proportional to $C_q\exp[-(\varepsilon/\varepsilon_q)^q]$, where $q = 0.5, 1, 2, 3$; $C_q(q)$ and $\varepsilon_q(q)$ are coefficients depending on q. The calculations for radial ion motion were performed for a cylindrical probe at $a/\lambda_D = 1$, 10 and 100. The normalized values of I_e'', I_i'' and I_p'' as functions of the parameter $\eta = -V/T_{\rm eff}$ are given in figure 27 for hydrogen ions at Maxwellian ($q = 1$) and Druyvesteyn ($q = 2$) electron-energy distributions and different a/λ_D. Here, $T_{\rm eff} = 2/3\langle\varepsilon\rangle$ is the effective electron temperature found as a corresponding integral of the EEDF and usually referred to as the electron temperature for non-Maxwellian EEDF.

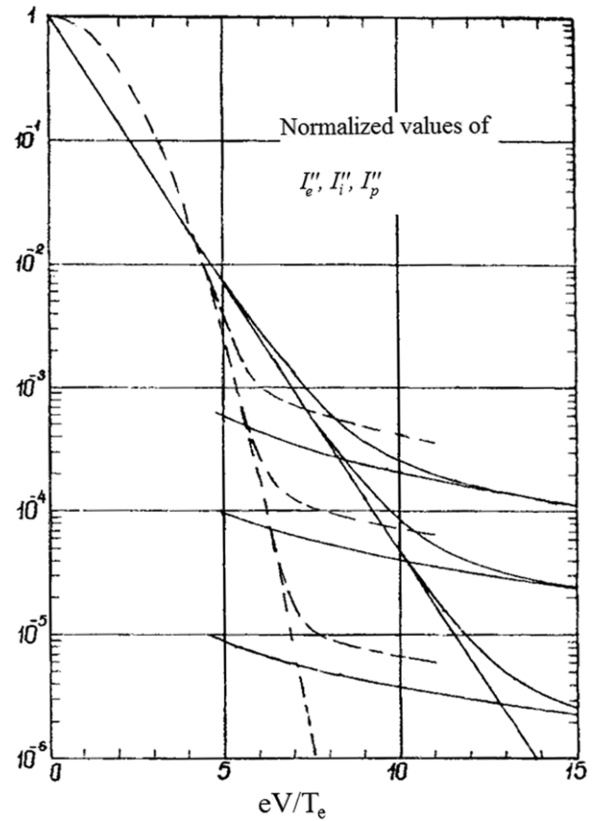

Figure 27. Normalized values of I_e'', I_i'' and I_p'' (absolute values) for the radial motion of protons at different ratios of $a/\lambda_D = 0.01$ (upper curves), 0.1 (middle curves) and 1 (lower curves) for Maxwellian (solid curves) and Druyvesteyn (dashed curves) distributions. For other ions, I_i'' is $(M/M_H)^{1/2}$ times less [89].

As seen in figure 27, at large electron energy, I_i'' for Druyvesteyn distribution is about twice as large as that for the Maxwellian distribution, whereas the opposite is true for the I_e'' values. Therefore, the dynamic range and energy span of EEPF (where I_i'' can be neglected) for Druyvesteyn distribution are less than that for Maxwellian distribution. For EEPF with $q = 0.5$, or for a bi-Maxwellian distribution typical in low-pressure CCP, the I_i'' effect is less than that for a Maxwellian distribution [89]. Shown in figure 27, the values of I_i'' for a more realistic case of $a/\lambda_D \geqslant 1$ are even less than that shown in figure 26 for the limiting case of $a/\lambda_D \ll 1$. The I_i'' values for non-hydrogen gases are $(M/M_H)^{1/2}$ times smaller than that given in figure 27. Therefore, in the majority of cases of EEPF measurement with a noise-limited dynamic range 50–70 dB, the effect of I_i'' can be neglected.

A popular method (implemented in many commercial probe-diagnostic instruments) to eliminate I_i'' is the subtraction from the total probe current $I_p(V)$ of the ion current $I_i(V)$ extrapolated from a large negative probe voltage (where $I_i \gg I_e$) to a lower probe voltage (where I_i and I_e are comparable). This procedure for the separation of the electron current (quite reasonable and justified in the classical Langmuir-probe routine) is (in our opinion) meaningless for the EEPF measurement and may even introduce more error.

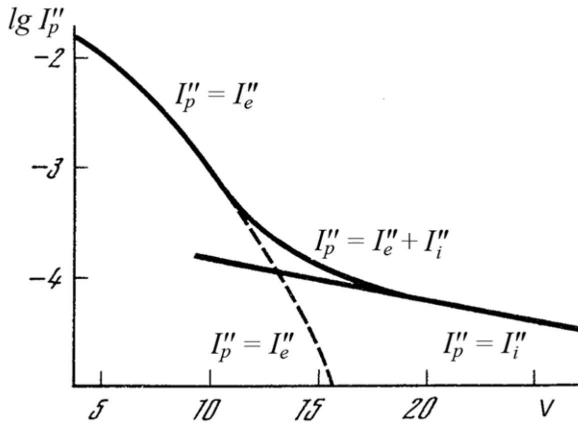

Figure 28. The procedure to correct the EEPF measurements affected by the ion current [12, 94].

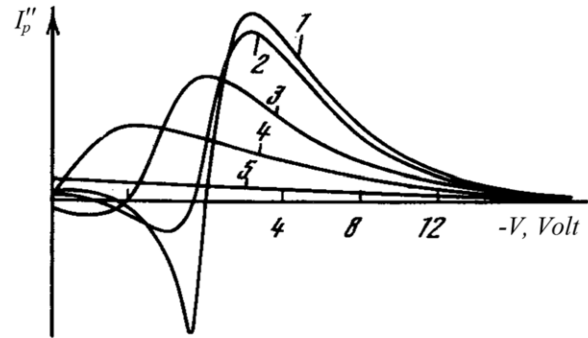

Figure 29. Influence of probe-surface contamination on I''_p (absolute values) in glow discharge in a mixture of neon and a 5% addition of benzyl. $pR = 1.2$ Torr cm, 20 mA discharge current [12, 97] . Hot probe (1), probe after heating termination at time 0 (2), 30 s (3), 60 s (4) and 120 s (5).

There are at least two reasons for this negative opinion. First, the extrapolation procedure is generally ambiguous. Second, the existing ion current $I_i(V)$ theories are not accurate enough to justify their application to account for the I''_i effect on EEPF. Suffice to say, the basic plasma parameters calculated according to these theories may be in error up to an order of magnitude [91–93]. The reason for the inaccuracy of the ion-current theories is that they do not account for many non-ideal conditions of the real plasma experiment, such as non-Maxwellian EEDF, unknown ratio of T_i/T_e, rare ion collisions that destroy ion orbital motion, ion drift velocity approaching $v_B \gg (T_i/M)^{1/2}$ caused by ambipolar field and failure of one-dimensional cylindrical sheath structures at highly negative probe voltages. At highly negative voltages, $I_p(V)$ can almost always be well fitted to a function proportional to $(-V)^{1/2}$. However, in contrast to popular belief, this fit does not prove the validity of the orbital-motion theory for the extrapolated $I_i(V)$ in a particular probe experiment. After all, due to the error-augmentation effect inherent to the differentiation procedure, a small error in $I_p(V)$ can lead to enormous error in I''_i.

A practical way to minimize I''_i error in EEPF measurement is the subtraction from the measured I''_p of the value of I''_p extrapolated from large probe voltage [94], where I''_p is apparently dominated by I''_i, as shown in figure 28. Of course, this technique has limited applicability and works in the electron-energy interval where I''_e and I''_i are comparable. Measurements with two probes having different radii allow the avoidance of the influence of I''_i on the measurement of EEPF [95, 96]. With this technique, the small probe provides accurate data for the low-energy part of the EEPF, whereas the thick probe (with $a/\lambda_D \gg 1$) has a negligible I''_i at large negative probe voltages, corresponding to the high-energy part of the EEPF. In the latter case, due to large I_p and I''_p signals, a relative reduction in internal apparatus noise can be achieved.

A problem in the described method may arise from the inability to obtain accurate measurements with the thick probe of the plasma potential needed to adjust the twice-measured EEPF. In this case, the adjustment of the two EEPFs can be performed in the middle-energy range where both probes give accurate measurement of I''_e.

A way to implement the two-probe technique could be to interchange the roles of the measuring and large RPs (in figure 4, P_1 and P_2). Note that the two-probe technique has limitations at high gas pressures, when the inequality $a[\ln(\pi l/4a)] \ll \lambda_e$ is not satisfied for the large probe. More information on the use of this technique in different gas-discharge plasmas can be found in [12].

3.6. Probe-surface effects

Probe-surface contamination is a long-recognized problem in probe diagnostics that has been studied in many works and is summarized in [10, 12, 19, 21, 25]. Therefore, we will briefly describe probe contamination and its effect on the quality of the measured EEPF, stressing the possible solutions to the problem with examples of EEPF measurements in chemically active plasmas.

Probe-surface contamination occurs in laboratory noble-gas plasma due to residual gases and, to a much larger extent, in plasma-chemical reactors with an intensive deposition of reaction products to the probe. The presence of a low-conductivity layer on the probe surface leads to a change in the probe work function and to an additional surface resistivity, contributing to the probe circuit resistance. The contaminated probe surface may also result in an increase in secondary electron–electron, electron–ion and electron photoemission. All of these effects may bring significant distortions into the measured EEPF and especially into its low-energy part.

An example of a dramatic probe-contamination effect on I''_p is shown in figure 29 for a dc glow discharge in argon with 5% of benzyl at a different time after probe heating at 900 °C [97]. The change in time of the voltage drop across the probe-contamination layer in pure argon-glow discharge is shown in figure 30 [98].

The change in the probe work function is a real problem in many published EEPF measurements, even in discharges in noble gases. Estimation shows that even at very low levels of residual gases, corresponding to a gas pressure of 10^{-6} Torr, a monolayer of residual gases appears on the probe surface in less than 1 min. It has been found that the probe work function is very sensitive to the probe temperature. The change in the probe current causes a temperature drift and, consequently, a change in its work function. This change results in probe

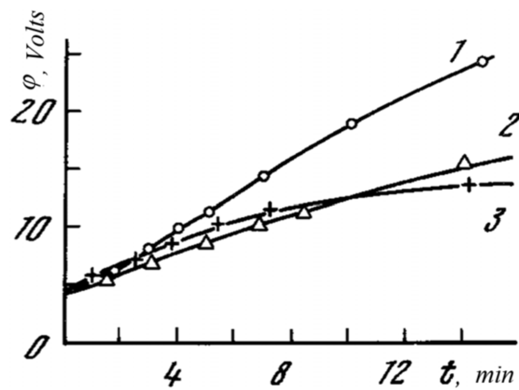

Figure 30. Variation of the effective probe work function in argon plasma. The probe material is molybdenum (1), tantalum (2) or tungsten (3) [98].

characteristic distortion because the probe-sheath voltage does not correspond to the applied probe voltage. As shown in [99], the change in the probe work function of the probe in mercury plasma can reach 1.5 V (close to the electron temperature in this experiment), with a minimal time constant τ_T of approximately 2 s. The change in the work function during the probe scan can be seen in the hysteresis of the probe characteristics and its derivatives obtained for different directions of the probe voltage change when the scan time τ_s is comparable to the probe temperature time constant τ_T. The hysteresis disappears in very slow ($\tau_s \gg \tau_T$) and at very fast probe scans. In the first case, the probe temperature (thus, its work function) is in equilibrium with the probe voltage and the probe characteristic and its derivatives are distorted. In the second case, due to thermal inertia, the probe work function remains constant during the probe scan and thus does not distort the probe characteristic and its derivatives.

It has been known for decades that the radical remedy to avoid distortion caused by changes in the probe work function is a fast ($\tau_s \ll \tau_T$) probe-voltage scan that can be achieved using a pulsed-probe technique with a scan-time order of ms [19]. To clean the probe between pulses of the scan voltage, a large negative (or positive) bias voltage is applied to the probe, as shown in figure 15. For a negatively biased probe, the cleaning is due to ion bombardment, whereas for a positively biased probe, the cleaning is due to probe heating by the electron current. Note that a fast-pulsed probe technique for EEPF measurement was used in the 1970s but has been mostly abandoned.

The cleaning of the probe by biasing should be done cautiously. The highly negative probe bias leads to probe sputtering, changing it size, especially for thin probes and dense plasmas. Therefore, in the pulsed repetitive regime, the negative probe bias (referenced to the plasma potential) should not exceed 50–100 V. Probe heating by electron current has the advantage of preventing polymer-film deposition on the probe, but the probe may accidentally be melted with excessive probe current. For this reason, hot probes are rarely used in experiments.

In some cases, the probe and its dielectric holder may be contaminated with a conductive layer of reaction products or with sputtered metal from other electrodes (such as rf electrodes in a low-pressure CCP) and from the probe itself during its cleaning by ion bombardment. A relatively simple solution to this problem can be a thin dielectric sleeve preventing electrical contact between the probe and its holder, as shown in figure 2.

Incorporating the considered above remedies to address the problems associated with the probe circuit resistance, low-frequency and rf plasma noise and change in probe work functions together with advanced analogue and digital electronic acquisition and processing routines in the probe-diagnostics systems described in [51, 55] resulted in the high-quality EEPF measurements shown in figures 8, 9, 11, 17, 18 and 19. However, the probe systems developed for basic plasma research and their commercial imitations still are not wholly suitable for reliable EEPF measurements in commercial and laboratory plasma-chemical reactors. Commercial plasma reactors (and some laboratory reactors) are not designed for plasma diagnostics, and attempts to directly apply probe instruments, proved in basic plasma experiments, are often frustrating.

There are many problems with implementing meaningful probe diagnostics in commercial plasma reactors: (a) large plasma rf potentials corresponding to the plasma source and rf-bias fundamental frequencies and their harmonics; (b) plasma low-frequency instability; (c) high rate of reaction-product deposition contaminating the probe surface, sometimes preventing even classical Langmuir-probe diagnostics; and (d) overly high impedance between the plasma and grounded chamber (mostly due to the limited surface of the conductive chamber area, its contamination, and/or dielectric protective coating).

Today, commercial plasma-simulation codes are the main tool for the study of plasma electrodynamics, transport and kinetics in commercial plasma reactors. These codes, when applied to plasmas in complex processing gas mixtures that involve molecular and electronegative gases and particles, are missing many cross sections for some plasma-chemical reactions. They also are missing some important effects of nonlocal and non-linear plasma electrodynamics that may even be dominant in rf plasma at low gas pressure [100]. In this situation, reliable EEDF measurements would give valuable experimental data for understanding the intricate processes in commercial rf plasma reactors and for validity testing of the corresponding numerical codes.

In an attempt to address the specific problems of EEPF measurements in chemically active plasma reactors with large amplitudes, wide spectra of rf noise and high deposition rate, the VGPS probe-diagnostic system [60] has been developed and tested in laboratory and commercial plasma reactors. Incorporating an automatic fast probe cleaning involving ion bombardment, rf biasing and forced probe heating by electron current allows for the reliable measurement of EEPF in plasma reactors with high deposition rates and significant noise.

An example of this measurement [101] given in figure 31 shows a snapshot of EEPF and plasma parameters from the display of the VGPS instrument. The measurement

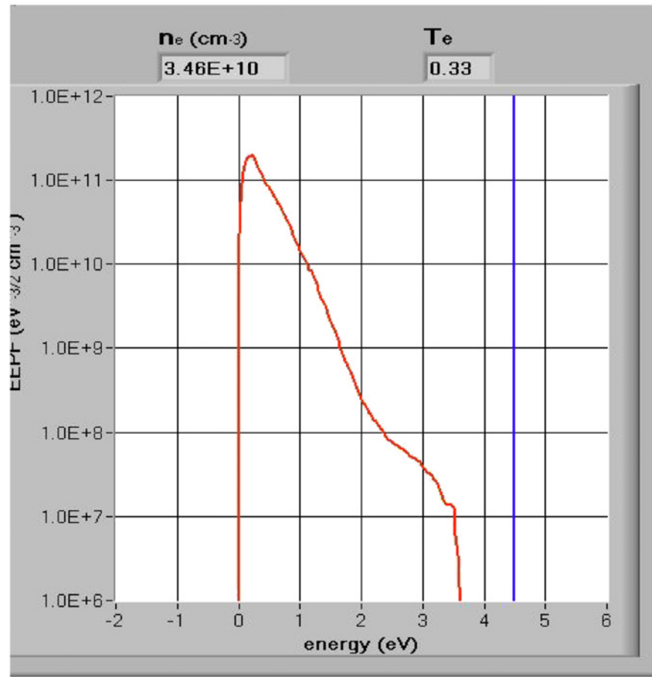

Figure 31. EEPF and plasma parameters measured in the microcrystalline-silicon-deposition plasma in a 2.45 GHz matrix-distributed ECR reactor [101].

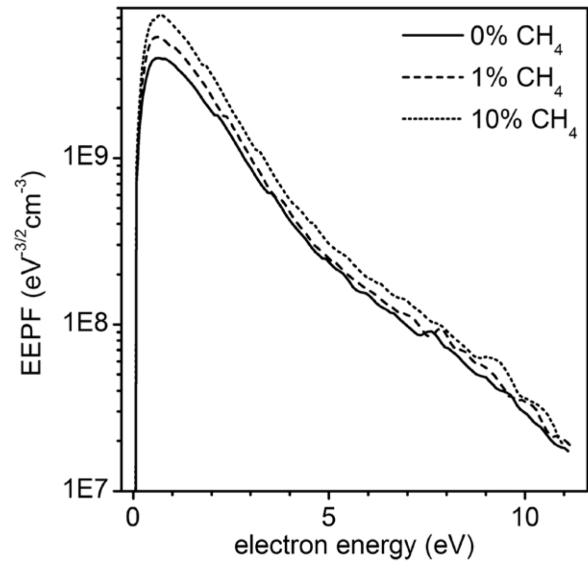

Figure 32. EEPF measured in the H_2/CH_4 ICP reactor with polymer-layer deposition at different contents of CH_4 [103].

was performed in a typical microcrystalline-silicon-deposition plasma in a 2.45 GHz matrix-distributed ECR reactor [102] driven at 1.5 kW and 10 mTorr of a gas mixture consisting of Ar, SiF_4 and H_2 with corresponding flow rates of 100, 15 and 150 sccm. Under these conditions, the deposition rate in the probe vicinity is 0.3 nm s^{-1} and the conventional Langmuir-probe measurement (without fast probe scan and continuous probe cleaning) has been considered to be impossible.

The EEPF displayed in figure 31 has three distinguishable parts. The bulk of the distribution, in the electron-energy interval between 0 and 2 eV and EEPF interval of 60 dB, corresponds to a Maxwellian distribution with an electron temperature $T_e = 0.33$ eV. Starting with $\varepsilon = 2$ eV, the EEPF slope changes (most likely due to the contribution of the second derivative of the ion current, mainly consistent of light hydrogen ions). After 3 eV, the EEPF sharply decreases due to the limited dynamic range of the measurement instrument. By extrapolating $I_p''(V)$ at large energy (assuming $I_p'' = I_i''$) to lower energy and subtracting it from the measured $I_p''(V)$, one can recover the EEPF in the energy range between 2 and 3 eV, thus extending the energy interval by 0.5–1 eV and the dynamic range of the recovered EEPF by 6–10 dB. The part of the EEPF with $\varepsilon > 3$ eV must be considered noise and removed from the EEPF.

Another example of the measurement of EEPF in an ICP plasma reactor with low-frequency instability and deposition of polymer layers in a 30 mTorr gas mixture of H_2/CF_4 is shown in figure 32 [103]. As one can see in figure 32, a measurement of EEPF with a dynamic range about 50 dB corresponding to the electron-energy interval of $7T_e$ is quite possible, despite the relatively high level of deposition and plasma instability.

3.7. Instrumental functions in probe measurements

In practice, because of various systematic errors, the measured EEPF $f_{pm}(\varepsilon)$ is always somewhat different from the real, nondistorted EEPF $f_p(\varepsilon)$ in plasma. Previously, we discussed how to design probe experiments to reduce the difference between $f_{pm}(\varepsilon)$ and $f_p(\varepsilon)$. However, systematic errors cannot be completely excluded. The influence of some spurious instrumental effects on the probe measurements of the EEPF can be described by applying so-called instrumental (or apparatus) functions [14, 21, 23, 25]. The result of measurements of the EEPF $f_{pm}(\varepsilon)$ is a convolution of the real EEPF $f_p(\varepsilon)$ and the instrumental function A:

$$f_{pm} = \int_{-\infty}^{\infty} f_p(x)A(\varepsilon - x)\,dx \equiv f_p * A. \qquad (17)$$

If there are n distortion effects, described by corresponding instrumental functions $A_1, A_2, \ldots, A_n$, then the function A is a convolution $A_1 * A_2 * \ldots * A_n$ and gives the full description of all included effects. As we see in equation (17), the instrumental function is reproduced by the measurement system when $f_p(\varepsilon)$ is a narrow (ideally δ-function) peak at a certain energy. The instrumental function shows how this peak is widened and distorted during the measurements. Accordingly, the distortion of the EEPFs of arbitrary form can be accounted for with equation (17).

Here are some important application features of the instrumental function that must be considered in processing probe measurements:

(1) The instrumental function allows the description of a number of (but not all) distortion effects by uniformly and conveniently taking them into account.
(2) The instrumental function A gives a full description of the distortion of the real EEPF by the included distortion effects. The correct result of measurements can be found as a solution of equation (17) (however, this problem

is ill-posed and may thus be accompanied by error augmentation, similarly to differentiation procedures).

(3) If the width of the instrumental function is finite and essentially smaller than an interval of substantial change in the EEPF $f_p(\varepsilon)$, the latter is well reproduced by $f_{pm}(\varepsilon)$.

(4) For a Maxwellian EEPF, $f_{pm}(\varepsilon)$ coincides with $f_p(\varepsilon)$, with the exception of the energies from 0 to the energies corresponding to the width of the instrumental function.

(5) Instrumental functions allow the comparison of measurement methods and the corresponding equipment and, thus, the choice of a method providing minimal distortion.

(6) If the EEPF has the property

$$\int_{\varepsilon_1-\Delta\varepsilon}^{\varepsilon_1} f_p(\varepsilon)\sqrt{\varepsilon}\,d\varepsilon + \int_{\varepsilon_2}^{\varepsilon_2-\Delta\varepsilon} f_p(\varepsilon)\sqrt{\varepsilon}\,d\varepsilon \ll \int_{\varepsilon_1}^{\varepsilon_2} f_p(\varepsilon)\sqrt{\varepsilon}\,d\varepsilon, \qquad (18)$$

where $\Delta\varepsilon$ is the half-width of the instrumental function and $\varepsilon_1 - \Delta\varepsilon \geqslant 0$, then the electron density in the energy interval from ε_1 to ε_2 can be found directly from $f_{pm}(\varepsilon)$ even if $f_p(\varepsilon)$ is significantly distorted (e.g. when $f_p(\varepsilon)$ has a sharp maximum). In this case, the form of the maximum can be strongly distorted during the measurements, but the area under the maximum still gives the correct electron density.

The various instrumental functions and their calculations for the Druyvesteyn method have been described in the literature [14, 21, 25, 104, 105]. Some describe the measurement methods of d^2I_p/dV^2 [48, 49, 106], whereas others illustrate the influence of the finite measurement time [21, 106]. A third group accounts for reflection and secondary emission of electrons from the probe surface [107, 108], and a fourth group accounts for oscillations of plasma potential [109]. As an example of practical application of instrumental functions, in [110] different methods of differentiation to obtain d^2I_p/dV^2 are compared.

The instrumental function of a d^2I_p/dV^2 measurement arrangement can be found by probe substitution with an electrical circuit having the second derivative of its volt/ampere characteristic close to a δ-function. An example of such a circuit used in the measurement of instrumental function in the commercial probe system SMARTProbe® is shown in figure 33. The measured instrumental function A of SMARTProbe®, working in the boxcar mode with a voltage sweep of 40 V, 1000 samples per point, 10 sweeps per scan and the voltage step of differentiation of 4 V, is shown in figure 34. In this example, the area under the measured d^2I_p/dV^2 is equal to 4.5×10^{-6} A V^{-1}, which defines the sensitivity of the system. The energy resolution of the system is about 4 eV. Note that the instrumental function found in this way characterizes the instrument but not the probe itself, which can be affected by an internal probe circuit resistance, probe contamination and secondary emission or electron reflection on the probe surface.

The combined instrumental function due to SMARTProbe® system convolution effect and that caused by the artificially introduced probe rf potential is shown in figure 34. The rf voltage with an amplitude of 2.5 V was introduced into the circuit shown in figure 33. As expected, the rf oscillations increase the width of the instrumental function

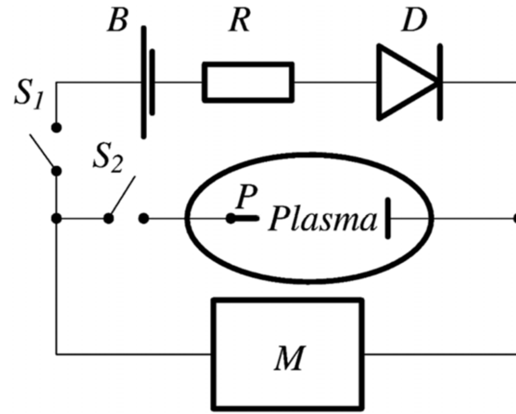

Figure 33. A circuit for simulating a narrow-energy group of electrons in a plasma. D is a diode, B is a dc source, R is a resistor, P is a probe and M is the measurement system. Switches S_1 and S_2 allow the probe circuit and/or the diode circuit to be connected to the measurement system M [111].

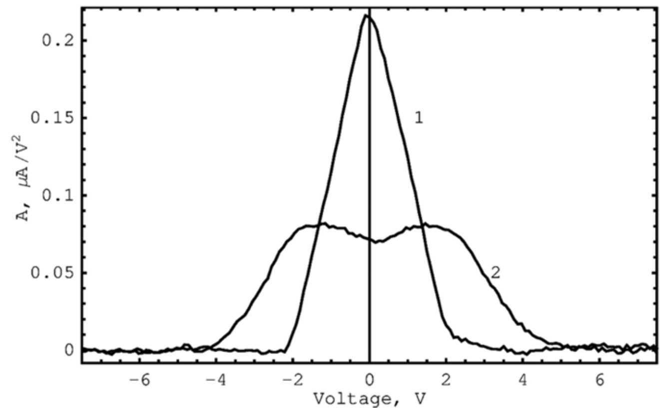

Figure 34. The measured instrumental function of the SMARTProbe®/ (1). The same function in the presence of potential oscillations with an amplitude of 2.5 V (2) [111].

(decrease the energy resolution) but do not change the system sensitivity (the area under measured curves remains the same). The above results are in good agreement with theoretical predictions [111].

To demonstrate how to determine the measurement sensitivity with real plasma, the probe measurements of d^2I_p/dV^2 obtained in the ICP afterglow plasma are shown in figure 35. The diode circuit has been included in the measurements, as shown in figure 33, via switch S_2. In this case, the sweep voltage was set to 10 V with 100 samples per point and 10 sweeps. For those conditions, the electron temperature in the plasma is 0.2 eV. With S_1 'open' to remove the diode circuit, no additional peaks are observed in the measured d^2I_p/dV^2 (dots). After connecting the diode circuit with a dc source B of 7.3 V, an additional maximum is seen in d^2I_p/dV^2 (solid line). Changing the R value allows for the variation of the area under this maximum. In figure 35, the additional artificial maximum on the d^2I_p/dV^2 curve is shown by an arrow. In this case, the artificially created maximum in d^2I_p/dV^2 (with R = 220 kΩ) gives an artificial 'density' $N_e = 5\times10^6$ cm^{-3} (note there is a misprint in [111] for N_e and the system sensitivity). Increasing R allows the determination

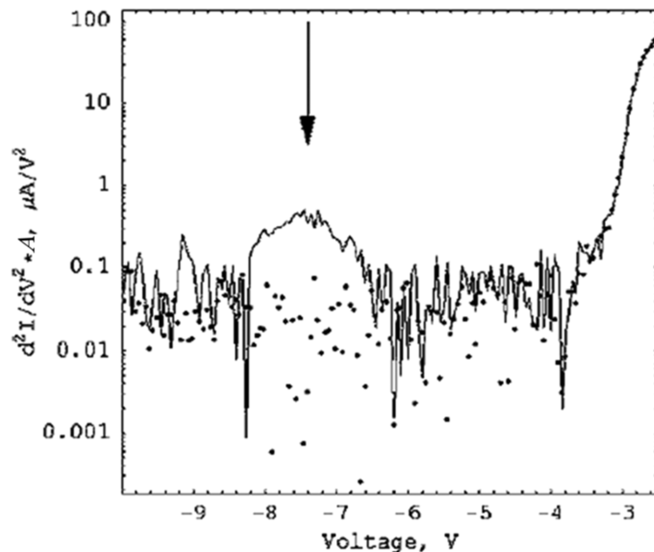

Figure 35. Measured EEDs in argon-rf-afterglow plasma without (dots) and with (solid line) an additional artificial maximum (indicated by arrow). The curves coincide for slow electrons. The gas pressure is 30 mTorr, the repetition frequency is 400 Hz, and the time after current interruption is 0.7 ms [111].

of the ultimate sensitivity of the measurement device. In this particular case, it is $2 \times 10^6\,\text{cm}^{-3}$. Thus, the simple circuit consisting of a diode, a resistor and a dc voltage source allows the determination of the instrumental function and the sensitivity of the particular differentiation instrument for a more detailed characterization of a probe-measurement device.

Another method of measuring instrumental functions includes all effects associated with the measuring system, the effects associated with probe itself and different distortion effects considered previously. For this purpose, the EEPF in a plasma with mono-energetic (but isotropically distributed) electrons should be measured [108]. One example of such a plasma is an afterglow plasma. In this case, a group of mono-energetic electrons arises in plasma-chemical reactions, such as Penning ionization of excited metastable atoms by collisions with other (excited) atoms. The results of such measurements in neon and xenon afterglows are shown in figures 36 and 37. In figure 36, the measurements were performed with a clean molybdenum probe. The cleaning was performed by ion bombardment of the probe surface. In figure 36, the measured instrumental function (solid line) is very close to the theoretical one (dashed line 2), which indicates that the reflection and/or secondary emission of the electrons from a clean probe surface are negligible. In the same figure, the theoretical curves with variation of the reflection coefficient are also shown. Figure 37 shows similar measurements with the probe having not been cleaned for a significant amount of time. The reflection and/or secondary emission are essential for dirty probes, producing negative parts of the instrumental function. These measurements demonstrate a harmful effect of reflection and/or secondary emission on the EEPF measurements, again confirming the necessity of probe cleaning during EEPF measurements even in noble-gas plasmas.

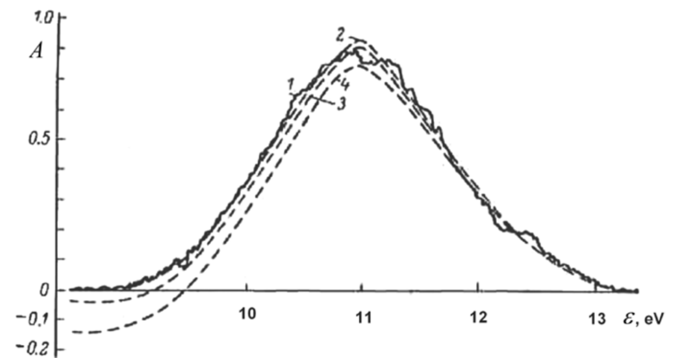

Figure 36. Instrumental function $A(\varepsilon)$ measured in a neon-afterglow plasma (1). The calculated function for the 'clean' probe (2). The calculated function for a probe with electron reflection at reflection coefficients of $1 - 0.016\,\text{V}^{-1}$ (3) and $1 - 0.056\,\text{V}^{-1}$ (4) [108].

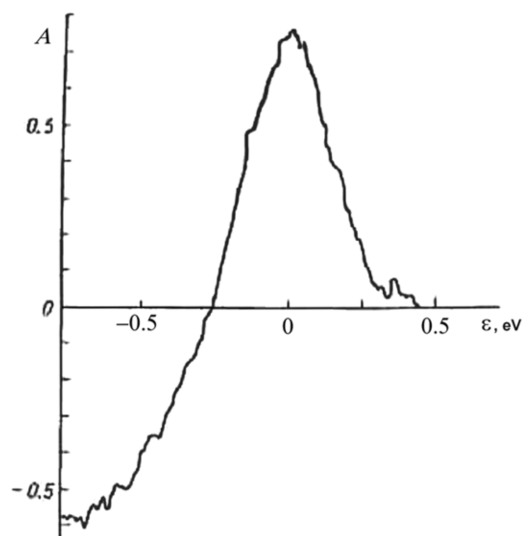

Figure 37. An instrumental function obtained from a probe with a dirty surface [108].

4. More complex plasma: beyond the limitations of the Druyvesteyn method

In basic plasma research and in some industrial applications, there are situations where the use of the Druyvesteyn formula in its classical form is not valid. The following section describes EDF-measurement methods in plasmas with higher gas pressures, substantial magnetic fields and anisotropy. The elements of electron-spectroscopy analysis will be discussed at the end of the section.

The currently existing probe theories allow, in principle, EDF measurements for the above conditions. However, measurement techniques based on these theories have not found broad applications. As a result, these techniques have not been studied to the same extent as the Druyvesteyn method; they are less developed, and their complete verification has not yet been completed. Therefore, this review cannot provide the same completeness in technical details for the measurements. Nevertheless, we will present the results of available efforts on EDF measurement in non-traditional (for the Druyvesteyn

method) plasmas to demonstrate their potential value and to challenge our colleagues to exert more effort into the development of EDF-measurement techniques applicable to these plasmas.

4.1. Higher pressures (plasmas with near-probe collisions)

In the case of elevated gas pressures, when electron collisions with other plasma particles in the near-probe plasma region become essential and inequality (12) is not satisfied, the Druyvesteyn formula is, strictly speaking, invalid. The case when $\lambda_e \approx a$ has been considered in [10, 114, 115]. It has been shown that distortions inflicted by collisions in the measured EEPF are more important for its low-energy part and that they can be accounted for by the application of a regularization procedure. The regularization formalism has been developed in [114] for a spherical probe. For a more practical cylindrical probe, the following integral equation, coupling the measured EEPF $f_{pm}(\varepsilon)$ with the real EEPF undistorted by collisions, $f_p(\varepsilon)$, has been derived in [115]

$$f_{pm}(\varepsilon) = f_p(\varepsilon)\left[1 - 2\int_\varepsilon^\infty \frac{\Psi_s f_p(x)\,dx}{x f_p(\varepsilon)[1 + \Psi_s(1-\varepsilon/x)]^3}\right], \tag{19}$$

where Ψ_s is the sink parameter

$$\Psi_s \approx \frac{4a}{3\lambda_e}\ln\frac{l}{2a}. \tag{20}$$

Finding the true EEPF, $f_p(\varepsilon)$ requires a deconvolution procedure with equations (19) and (20) using an iteration technique. For a weak collision effect, when $\Psi_s \ll 1$, the true values of plasma density N and electron temperature T_e can be found through integration of the measured $f_{pm}(\varepsilon)$ (to get N_m and T_{em}) and correction according to expressions

$$N \approx N_m(1 + 4\Psi_s/3) \tag{21}$$

and

$$T_e \approx T_{em}(1 - \Psi_s/2). \tag{22}$$

For higher pressures, when $\lambda_e \ll a[\ln(\pi l/4a)] \ll \lambda_\varepsilon$, the problem was solved in [116]. Here, λ_ε is an electron-energy relaxation length (more details on the energy relaxation length can be found, e.g., in [25]). The theory [116] is valid for gas pressures when there are many collisions in the plasma volume disturbed by the probe ($\lambda_e \ll a[\ln(\pi l/4a)]$), but electrons from undisturbed plasma reach the probe surface practically without the loss of the total (kinetic and potential) energy due to collisions ($a[\ln(\pi l/4a)] \ll \lambda_\varepsilon$). For atomic gases and weakly ionized plasma, λ_ε is on the order of $100\lambda_e$, and the theory thus allows for the expansion of the pressure range for probe measurements of the EEPF for typical probe dimensions up to several hundred Torr. It was demonstrated [116] that for thin (with respect to the probe radius) probe sheaths (sufficiently high electron density) or arbitrarily thick sheaths and $vD_e = \text{const}$ or $\lambda_e = \text{const}$ (e.g. in argon plasma), the following formula can be used to infer the EEPF:

$$f_0(\varepsilon = eV) = -\frac{3m^2 a\ln(\pi l/4a)}{8\pi\lambda_{e(\varepsilon=eV)}Ve^3S_p}\frac{dI_e}{dV}. \tag{23}$$

Here, D_e is the electron diffusion coefficient.

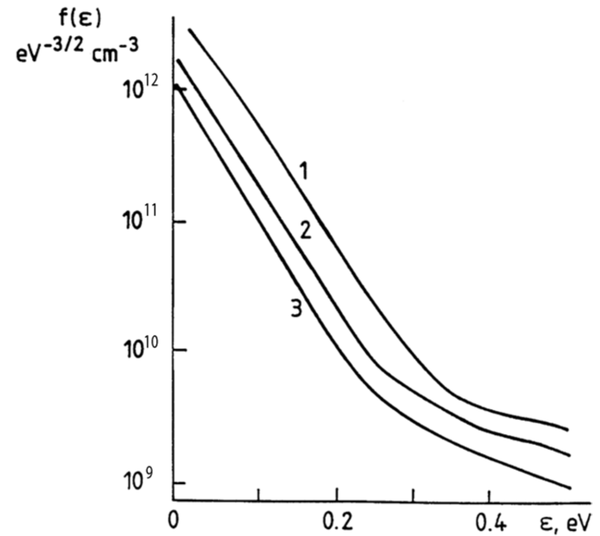

Figure 38. EEPF in a helium afterglow at different times τ with a probe having $a = 0.1$ mm, $l = 15$ mm and a gas pressure of 40 Torr: $\tau = 100\,\mu$s, $T_e = 0.047$ eV (1); $\tau = 300\,\mu$s, $T_e = 0.044$ eV (2); and $\tau = 500\,\mu$s, $T_e = 0.043$ eV (3) [120].

This method simply requires the measurement of dI_p/dV and therefore may be referred to as the first-derivative method. If sheath is thick but vD_e is not a constant, then the simple formula (23) generally cannot be used and it is necessary to know the potential profile in the probe sheath, which can be found in principle from the Poisson equation jointly solved with the equation of motion of the ions in the sheath. Formula (23) has been used in practical measurements of the EEDFs, for example, in [116–120]. An example of the measurements is shown in figure 38 [120].

A more general nonlocal probe theory, which is valid for $\lambda_\varepsilon \gg a[\ln(\pi l/4a)]$ and thus includes both collisionless and collision cases, was developed in [120, 121]. The developed theory gives expressions that are somewhat similar to (19) and (20). In this case, the electron current to the probe is

$$I_e = \frac{8\pi e S_p}{3m^2}\int_{eV}^\infty \frac{(\varepsilon - eV)f_0(\varepsilon)\,d\varepsilon}{\gamma + (1 - eV/\varepsilon)\Psi(\varepsilon, V)}. \tag{24}$$

In this expression,

$$\Psi(\varepsilon, V) = \frac{1}{\lambda_e}\int_a^{\pi l/4} \frac{\sqrt{\varepsilon}D_e(\varepsilon)\,dr}{(r/a)\sqrt{\varepsilon - e\varphi(r)}D_e(\varepsilon - e\varphi(r))}, \tag{25}$$

$\varphi(r)$ is the plasma potential at distance r from the probe and γ is a factor of an order of unity which can be approximately given as $\gamma = 4/3 - 0.62\exp[-\lambda_e/(2a)]$ [25]. In equation (24) f_0 is the EDF in the undisturbed plasma.

For a thin probe sheath or arbitrarily thick sheath and $vD_e = \text{const}$, $\Psi = \frac{a}{\lambda_e}\ln\frac{\pi l}{4a}$. Apparently, this method is more difficult to implement because it requires the solution of the integral equation (24) to infer the EEPF from the measured electron probe current I_e. In practice, however, it may be more convenient to use the Druyvesteyn or the first-derivative methods because it is always possible to adjust the probe radius to satisfy the corresponding validity condition.

More details of the general nonlocal kinetic theory can be found in [21, 22, 24, 25, 27, 120]. In [21], an evaluation

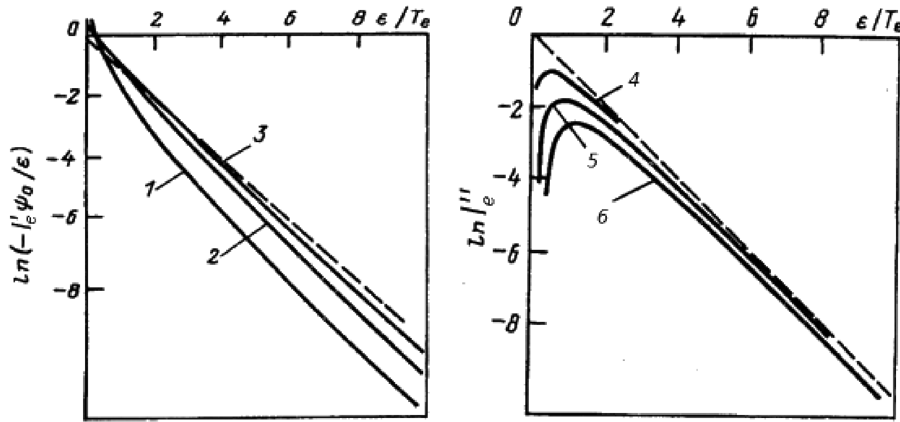

Figure 39. Calculated $\ln(-I_e''$ (right) and $\ln(-I_e'\Psi(\varepsilon)/\varepsilon)$ (left) for a Maxwellian EEPF, $\Psi = 1$ (1), $\Psi = 5$ (2), $\Psi = 20$ (3), $\Psi = 0.3$ (4), $\Psi = 1$ (5), $\Psi = 2$ (6), and the model Maxwellian EEPF (dashed line) [21].

of the validity limits of the Druyvesteyn and first-derivative methods based on the general theory has been performed. Many examples of EEDF distortion with the evaluation of measurement errors have been analysed. These errors depend on the specific form of the EEDFs. As an example, the results of calculations of electron probe current for Maxwellian EEPF, demonstrating deviation of the solution from ideal (a straight line), are shown in figure 39. It was shown that, for Maxwellian EEPF and $\Psi > 5$, an error in the obtained values of N and T_e using (23) is not more than 10%. Generally, it is possible to conclude [21] that the Druyvesteyn method is reasonably applicable if $\lambda_e > 0.75a\ln[\pi l/4a]$ and formula (23) may be used if $\lambda_e < (a/7)\ln[\pi l/4a]$.

For practical realization of the first derivative and more general nonlocal methods, the precautions to avoid the probe measurements errors considered in section 3 are relevant. It is clear that probe circuit resistance, probe-sheath rf oscillation and surface effects can distort the EDF measurement unless they are properly addressed in the probe measurement. For higher pressures (and magnetic fields described in the next subsection), it is unlikely to satisfy inequality (12) for the probe holder and it may create significant disturbances of the surrounding probe plasma. Therefore, the requirements for a good probe design may be even more important. Numerical analysis (similar to that done in [56]) and/or experiments with different sized probes [112] could contribute to the solution of the problem but require significant additional work. Comparative measurements with different probe and probe-holder sizes and orientations could be useful and are highly desirable to understand the proper probe design in collisional and magnetized plasmas.

An additional issue is the temporal resolution of the probe measurement at relatively high pressures and in the presence of a magnetic field. In those cases, the transport of electrons to the probe is slow due to the reduction by the electron diffusion caused by collisions and the magnetic field. This issue poses an additional restriction on the speed of the probe measurement [25]. The timescale for electron diffusion to the probe is $\tau_D = \Lambda_p^2/D_e$, which can be much larger than that defined by the probe-sheath capacitance for the collisionless probe regime. Here, Λ_p is the diffusion length of the plasma area distorted by the probe.

4.2. Magnetic fields

The measured EEPF in plasma with magnetic fields is of a great interest due to the importance of the magnetized plasma in laboratory and practical applications. In this case, for theoretical description of electron probe current, the electron Larmor radius R_{Le} is an important plasma parameter. The probe current also depends on the probe orientation with respect to the magnetic lines. The most interesting are two-probe orientations: magnetic field $\boldsymbol{B}$ is parallel to the probe and $\boldsymbol{B}$ is perpendicular to the probe. In the presence of weak magnetic fields ($R_{Le} \gg l$, for parallel probe and $R_{Le} \gg a$, for perpendicular probe) the Druyvesteyn method is still valid and can be used without correction [5]. Increasing the magnetic field is somewhat similar to increasing the gas pressure; therefore, an approach similar to that described in the previous section can be used [21, 22, 24, 25, 27, 116].

It has been demonstrated that in a strong magnetic field ($R_{Le} \ll l$, $\boldsymbol{B} \parallel l$) and ($R_{Le} \ll a$, $\boldsymbol{B} \perp l$) for thin probe sheath ($a/\lambda_D \gg 1$) the following formulae are applicable:

for parallel probe ($\boldsymbol{B} \parallel l$) [21, 25, 116, 122]

$$f_0(\varepsilon) = -\frac{3\omega_H m^{5/2}}{64\sqrt{2}\pi e^2 a(eV)^{3/2}}\frac{\mathrm{d}I_e}{\mathrm{d}V}, \qquad (26)$$

for perpendicular probe ($\boldsymbol{B} \perp l$) [25, 122]

$$f_0(\varepsilon) = -\frac{3m^2\ln(\pi l/4a)}{16\pi^2 e^3 V R_{Le}}\frac{\mathrm{d}I_e}{\mathrm{d}V}. \qquad (27)$$

Here, ω_H is the electron cyclotron frequency. Figure 40 shows the first derivative to the probe characteristic, $\mathrm{d}I_p/\mathrm{d}V$, measured with a parallel and a perpendicular probe under the same plasma conditions [122]. Measurements have been performed in the toroidal plasma device 'Blaaman' [123]. It is possible to see that $\mathrm{d}I_p/\mathrm{d}V$ measured by the parallel probe is essentially smaller than that for a perpendicular probe. Figure 41 shows the EEDFs measured in [124].

The general nonlocal kinetic theory, similar to that discussed for higher pressure plasma in the previous section, has also been developed for the magnetized plasma diagnostics in [120, 121]. It gives exactly the same expression (24) for

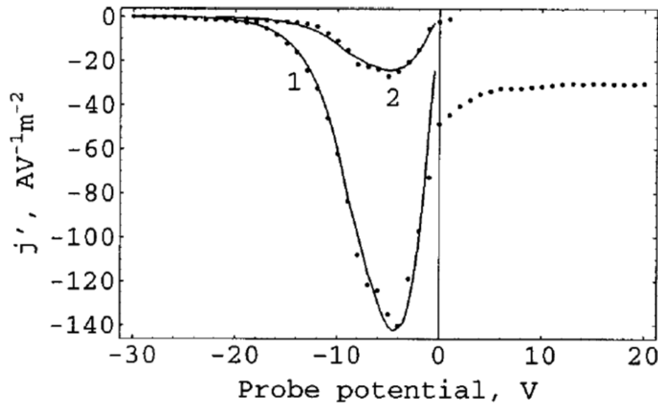

Figure 40. Measured (dots) and calculated (line) I_e' in a magnetized plasma for perpendicular (1) and parallel (2) probes [122].

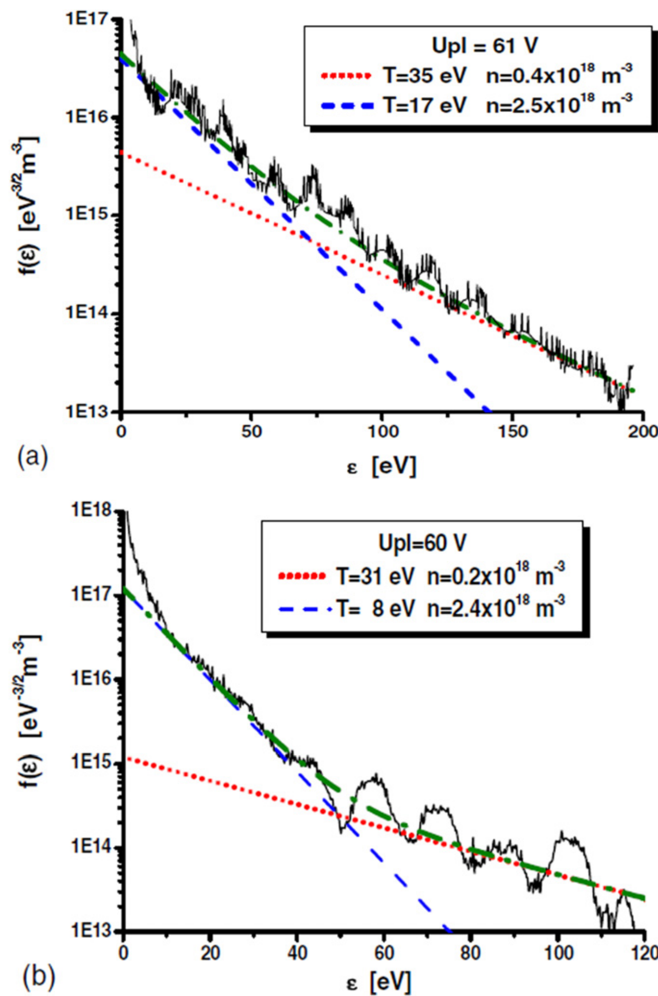

Figure 41. The EEPF obtained by a perpendicular (*a*) and parallel (*b*) probes (solid curves) and the CASTOR tokamak edge plasma. Magnetic field $B = 1.3$ T. The dashed—dotted lines are the bi-Maxwellian approximation. The dashed line represents the distribution of the low-energy electron population; the dotted line is that of the high-energy population. The dashed—dotted line is the sum of the dotted and dashed lines [124].

electron probe current with $\Psi_\perp = a\ln(\pi l/4a)/\gamma R_{\mathrm{Le}}$ for the perpendicular probe and $\Psi_\parallel = \pi l/4\gamma R_{\mathrm{Le}}$ for the parallel probe. This theory has been also applied to the interpretation of the measurements (e.g. in [124, 125]).

However, the accuracy of this theory is still unclear and requires additional studies. For example, the theory uses the same approach to a boundary conditions as that for the above higher pressure probes. However, the trajectories of electrons between collisions are not straight lines but arcs, which could be a source of unknown error. Therefore, it is probably more reasonable to use the Druyvesteyn or first-derivative methods in practice because it is almost always possible to adjust the probe radius and use different probe orientations to satisfy the corresponding validity condition. An analysis similar to that performed for the high-pressure probe suggests that the Druyvesteyn method is reasonably applicable if $\Psi_\perp, \Psi_\parallel < 0.75$ and formulae (26) and (27) if $\Psi_\perp, \Psi_\parallel > 7$.

For practical measurements, the above remarks from the previous subsection should be considered. Because the diffusion of charged particles to the probe holder can be essential, it is advisable to place it perpendicular to the magnetic field. Additionally, for magnetized plasma, the timescale of diffusion to the probe is of the order of $\frac{3a^2\omega_{\mathrm{H}}^2}{8v^2\nu}$. This expression gives, for example, the following restriction on the application of a fast-sweep probe [113] for the exploration of magnetized plasma oscillations [25]:

$$\frac{3a^2\omega_{\mathrm{H}}^2}{8v^2\nu T_{\mathrm{e}}}|eV_{\mathrm{sw}}| \ll \tau_{\mathrm{sw}} \ll \tau_{\mathrm{fl}}, \tag{28}$$

where V_{sw} is the voltage range of the sweep, τ_{sw} is the sweep time and τ_{fl} is the typical fluctuation time. In real experiments, taking into account that the probe should be fast enough to resolve oscillations, this condition may be difficult to satisfy.

4.3. Anisotropy

The issue of the EDF in anisotropic plasmas is reviewed in [19, 21, 25, 27]. In this subsection, we give an abbreviated review of the methods for evaluation of an anisotropic EDF, which can be useful for probe diagnostics with very low gas pressures and/or strong electric fields. Unfortunately, a full recovery of the anisotropic EDF requires a rather complicated experimental probe design (flat one-sided probe placed in an anisotropic plasma under a number of different angles known with high precision) and a cumbersome numerical recovery procedure. Therefore, the wide application of a flat one-sided probe is questionable. Sometimes, it is possible to use a simple cylindrical probe placed in the plasma under a number of angles, which can give an insight into the degree of EDF anisotropy and provide some details of the EDF. A spherical probe can still measure the EEDF (but not the full EDF) in the anisotropic plasma, providing that some additional conditions are satisfied. Of course, information about the angle distribution in such a measurement is completely lost.

It has been demonstrated [5, 25] that, for the spherical probe, the Druyvesteyn method in collisionless anisotropic plasma is valid in two cases: the probe sheath is thin (which implies sufficiently high electron density) and the probe sheath is arbitrarily thick but spherically symmetric. Note here that the spherically symmetric sheath occurs in partially anisotropic plasma when the plasma contains a high-energy low-density flux of electrons with an isotropic electron background. The

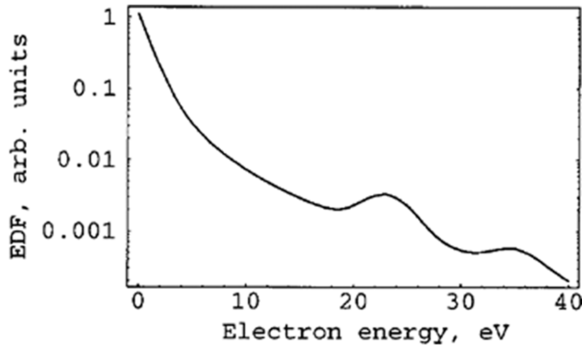

Figure 42. The EEPF in a low-pressure (0.1 Torr) hydrogen constricted arc plasma at the discharge axis.

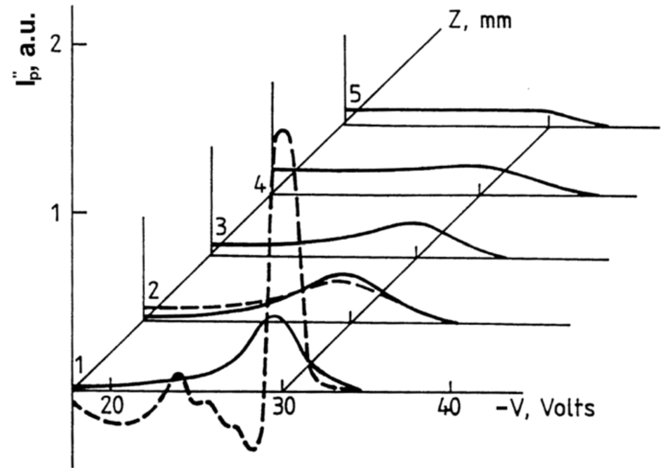

Figure 43. I_p'' with respect to the potential V measured at the discharge axis at a distance Z from the cathode by probes in two mutually perpendicular orientations. At $Z > 2$ mm, I'' is the same for both probes and is proportional to EEPF. The helium pressure is 2.3 Torr, the discharge current is 0.5 A, the electron density is 1.1×10^{11} cm^{-3} [30].

negligible effect of the fast electrons on the probe-sheath geometry is due to the fact that the Debay length and potential distribution in the probe sheath are defined by the low-energy part of the EDF [90]. The measurements of an anisotropic EEPF with a spherical-probe method were performed in the study of constricted discharges [126, 127]. Figure 42 represents the EEPF obtained in a low-pressure (13 Pa) hydrogen constricted arc discharge. The two peaks in the measured EEPF at 22 and 35 eV are due to electron acceleration by a double-layer structure in the constricted region of the plasma [126].

Measurements with cylindrical probes provide some information about anisotropic EDF [128, 129]. In this case, rotation of the probe perpendicular to its axis can actually indicate the presence of the anisotropy. Due to the symmetry of the spherical functions Y_j^k, measurement with a cylindrical probe can determine only the even coefficients f_j^k in the expansion (2). Let us assume that plasma has axial symmetry (in this case, $k = 0$, $f_j \equiv f_j^0$ and $P_j \equiv Y_J^0$ are the Legendre polynomials) and that the probe sheath is thin. The measured probe current depends on the probe orientation. Let the axis of the probe have an angle Φ_c to the axis of the plasma symmetry. Then the second derivatives of the probe electron current is

$$\frac{d^2 I_e}{dV^2} = \frac{4\pi e^3 al}{m^2} \sum_{j=0}^{\infty} F_{2j}(eV) \int_0^{\pi} P_{2j}(\sin\theta' \sin\Phi_c)\, d\theta'. \tag{29}$$

Here, θ' is a polar angle of a normal to some element in a auxiliary coordinate system which has a polar axis normal to the plane containing the symmetry axis of the plasma and the probe, and

$$F_{2j}(eV) = f_{2j}(eV) - \int_{eV}^{\infty} f_{2j}(eV) \frac{\partial}{\partial(eV)} P_{2j}\left(\sqrt{\frac{eV}{\varepsilon}}\right) d\varepsilon. \tag{30}$$

Thus changing Φ_c, it is possible to obtain a system of equations for finding f_j. However, the equations contain the coefficients f_j with even j alone. Therefore, this method does not give us complete information about the EDF. This method has been used for the measurements of the EDF in the near-cathode region of low-pressure arc discharges [30, 128].

Experimental results on I_p'' measured at the axis of a low-pressure (280 Pa) helium discharge with probes perpendicular (dotted curve) and parallel (solid curve) to the discharge axis at a distance z from the cathode are shown in figure 43 [30]. For $z > 2$ mm, the curves practically coincide, and I_p'' is proportional to f_p. As one can see in figure 43, the relaxation of the cathode beam (no difference in the measurements made by the differently oriented probes) occurs at the distance of $z > 2$ mm. The method considered above can be used for EDF diagnostics in axially symmetrical partially anisotropic plasmas where the probe sheath satisfies cylindrical symmetry.

A more sophisticated (but technically more complicated) method, suitable for measurements of EDF with an arbitrary degree of anisotropy, has been developed in [130–132]. In this method, the measurements are performed with a flat one-sided probe having different angle positions referenced to the main anisotropy direction. For the case of cylindrically symmetric plasma, to infer the EDF from the probe measurement, the procedure developed in [130] should be applied, whereas for plasma with arbitrary anisotropy, the formalism developed in [131] must be applied. For all cases, the probe sheath must be thin.

Let consider in more detail the case of the cylindrically symmetric plasma typical for a plasma experiment. The main formula of the method defining the coefficient $f_j = f_j^0$ of the expansion (2) is

$$f_j(eV) = \frac{(2j+1)m^2}{4\pi e^3 S_p} \int_{-1}^{1} (I_e''(V, \cos\Phi_f) + \int_{eV}^{\infty} I_e''(\varepsilon, \cos\Phi_f) R_j(V, \varepsilon)\, d\varepsilon) P_j(\cos\Phi_f)\, d(\cos\Phi_f). \tag{31}$$

Here, Φ_f is the angle between the plasma symmetry axis and the normal direction of the probe conducting surface,

$$R_j(\varepsilon, V) = \frac{2^{-(j+1)}}{eV} \sum_{k=0}^{[\frac{j}{2}]} a_{kj} \left(\frac{\varepsilon}{eV}\right)^{\frac{j-2k-1}{2}}, \tag{32}$$

where

$$a_{kj} = (-1)^k \frac{(2j-2k)!(j-2k)}{k!(j-k)!(j-2k)!} \tag{33}$$

and

$$\left[\frac{j}{2}\right] = \begin{cases} \dfrac{j-1}{2}, & \text{for odd } j; \\ \dfrac{j}{2}, & \text{for even } j. \end{cases} \tag{34}$$

From (31), for example, we obtain for f_0

$$f_0 = \frac{m^2}{4\pi e^3 S_p} \int_{-1}^{1} I_p''(V, \cos\Phi_f)\, d(\cos\Phi_f). \tag{35}$$

Thus, it is necessary to measure I_p'' for different Φ_f and to calculate expression (35) to determine f_0 and expression (31) to determine of f_j. A study of errors, arising during the EDF measurements by a flat one-sided probe, was performed in [132].

Formulae (35) and (31) are valid for any degree of plasma anisotropy. To increase the accuracy in strongly anisotropic plasma, it is necessary to conduct measurements for a rather large number of different angles Φ_f. The considered method has been used, for example, for measurements of the drift velocity as a function of electron energy in noble-gas plasma discharges [133] and to study the momentum relaxation of the electrons fluxes [134]. The energy dependence of the coefficients f_j measured in a low-pressure (65 Pa) helium dc positive column for discharge current 0.5 A is shown in figure 44 [133]. In this rather high-pressure plasma, the measured anisotropy degree is very small, and the conventional Druyvesteyn method is quite applicable. The accuracy of the inferred EDF depends on the number K of the measurements performed at different angles. Figure 45 shows the reproduction of the model function by calculated EDF for different numbers of probe orientations K. As expected, increasing the number of measurements at different angles and, thus, the number of coefficients f_j leads to a more accurate EDF recovery.

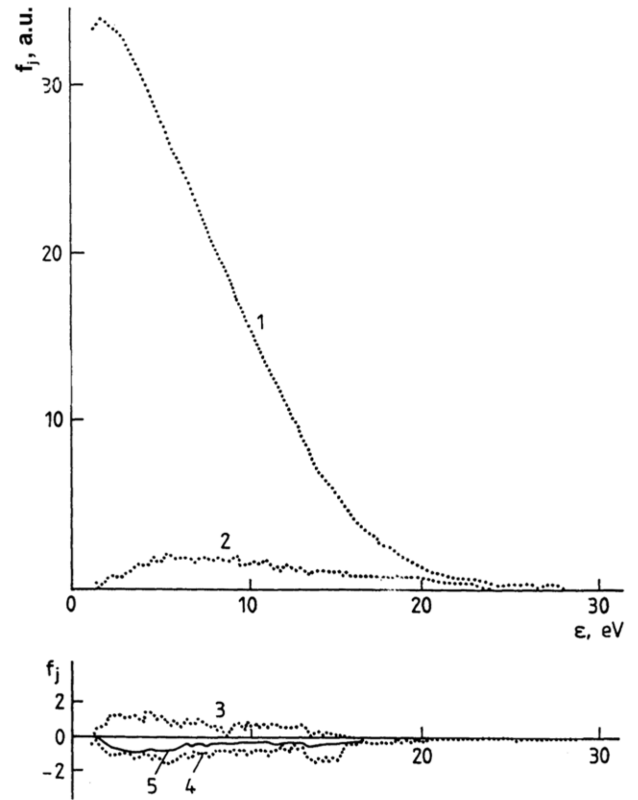

Figure 44. Coefficients f_j in a helium low-pressure (0.5 Torr) positive column: f_0 (1), f_1 (2), f_2 (3), f_3 (4) and f_4 (5) [134].

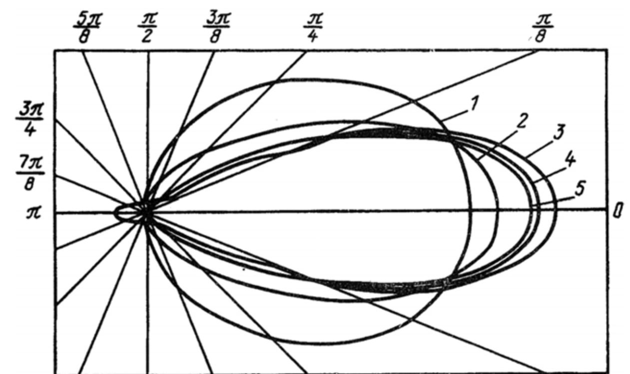

Figure 45. The polar diagram EDF for electrons calculated for different numbers of probe orientations K: $K = 3$ (1); $K = 5$ (2); $K = 7$ (3); $K = 9$ (4); model function (5) [21].

4.4. Plasma electron spectroscopy

The sensitivity, dynamic range and energy resolution of current EDF measurement techniques allow for the analysis of the fine structure in the EDF tail corresponding to a tiny fraction (10^{-3}–10^{-6}) of the electron population. Such sensitivity in the EDF measurement allows the recognition and evaluation of some plasma-chemical and collisional processes that affect the EDF structure. This method, called plasma electron spectroscopy (PLES), is based on the measurement of the EDF in the conditions where a part of the distribution function is affected by a particular collisional process. In this case, the EDF structure can be a source of information about such a process. Usually, such analysis is possible when the contribution of thermal electrons to the tail of the measured EDF is minimal and does not mask the EDF structure caused by the particular collisional process. Such conditions are achieved at low electron temperatures, when EDF drops sharply with electron energy. The idea of PLES has been realized in experiments with afterglow plasma [21, 25, 32] where the EEDF consists of two almost non-interactive groups of electrons. Low-energy groups of thermal electrons with Maxwellian distributions have electron temperatures at the order of 0.1 eV. The distribution of energetic electron groups is far from equilibrium and exhibits several peaks in the EDF tail. The density of these electrons is from 10^4 to 10^6 times less than that of the low-energy electrons. The origination of the high-energy electrons is collisions of metastable excited atoms between themselves and with electrons in the reactions

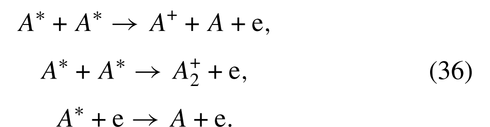

$$\begin{aligned} A^* + A^* &\to A^+ + A + e, \\ A^* + A^* &\to A_2^+ + e, \\ A^* + e &\to A + e. \end{aligned} \tag{36}$$

Here, A^* denotes an exited atom, and A^+ and A_2^+ denote atomic and molecular ions. The first two reactions in (36) represent the Penning ionization process, whereas the third describes the super-elastic collision of an exited atom with a low-energy thermal electron.

Analysis of the measured EDF structure allows the determination of information about the spectra and the rate constants of the corresponding reactions (36). A detailed analysis of the relationship between the measured EEDF structure and the reaction-rate constant is provided in [32]. A similar method has been studied in [135] for the measurements of the reflection coefficients of electrons from plasma boundaries and for the energy dependence of the frequency of electron–electron collisions.

The authors of [136] appear to be the first to suggest and use the PLES method to monitor and control the absolute component densities of a gas mixture. For this purpose, the exact knowledge of EEDF may not be as important because a calibration of the system can be provided independently.

Recently, it was demonstrated that the plasma of a dc glow discharge near a cold cathode, where T_e can be close to room temperature, can also be suitable for PLES and analytical gas detection [137]. The EEDF measurement in a dc glow discharge is considerably simpler and has dramatically higher sensitivity than that in the afterglow plasma. For this reason, a short (without positive column) dc discharge with a cold cathode and a wall probe has been used experimentally [137] for PLES analysis. Here, the EEDF was measured with a negatively biased wall probe collecting only high-energy electrons. The area of the wall probe is significantly larger than that of the cylindrical Langmuir probe. The large wall-probe surface area results in a dramatic increase in the probe sensitivity. The distortion of the EEDF measurements associated with the ion current effect is significantly reduced due to the large wall probe radius. Consequently, the ion current to the wall probe is practically independent of the probe voltage.

It is worth noting that, due to the use of a wall probe, the discharge volume (and device) size in an implementation of PLES can be dramatically reduced because there is no need for an insertion of a cylindrical Langmuir probe into the plasma. This fact opens a possibility of building a micro-discharge operating at atmospheric gas pressure as a micro-scale gas sensor.

In [137], the discharge takes place between a plane disc-shaped molybdenum cathode (C) and anode (A), schematically shown in figure 46. The plasma volume is bounded by a cylindrical stainless steel wall (W). The cathode and anode are 2.5 cm in diameter. The distance between the cathode and anode is 1.2 cm. The wall W was used as a large wall probe. The discharge plasma contains energetic primary electrons accelerated in the near-cathode sheath in the direction of the anode. These electrons ionize the gas thus producing the plasma. They also create excited and metastable atoms, which can in turn generate other groups of energetic electrons, such as in reactions (36).

The maxima in d^2I_p/dV^2 measured with the wall probe in the glow discharge plasma in neon, argon and oxygen

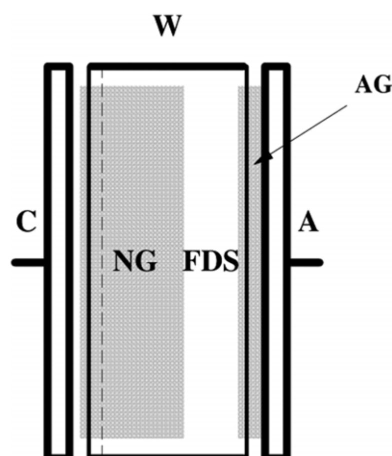

Figure 46. Schematic diagram of an experimental device with a cold cathode (C), an anode (A), and a cylindrical wall (W). A typical structure of the discharge plasma is shown. The dashed line indicates the cathode-sheath boundary. The negative (NG) and anode (AG) glows are the shaded regions near the cathode and anode, respectively, and the Faraday dark space (FDS) is between the NG and AG [135].

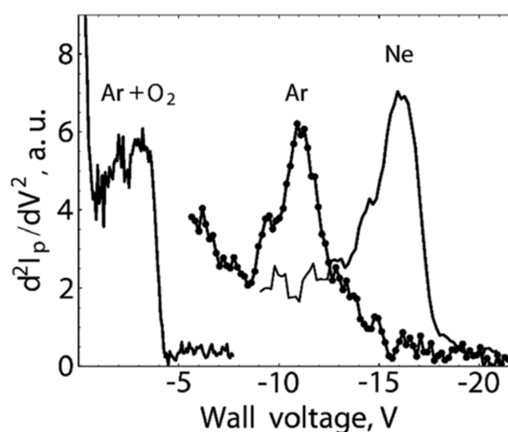

Figure 47. High-energy portion of d^2I_p/dV^2 (absolute value) in neon (3 Torr), argon (0.5 Torr) and oxygen (20%)/argon (80%) (0.5 Torr) dc discharge. The discharge currents were 10 mA, 2 mA and 3 mA, respectively. The maxima at 16 eV and 11.5 eV are due to collisions of neon and argon metastable atoms with slow electrons. The maximum at ≈4 eV is due to electron detachment from oxygen, i.e. $O^- + O \rightarrow O_2 + e$ [137].

(20%)/argon (80%) mixture are shown in figure 47. the peaks in the d^2I_p/dV^2 energy dependence for pure neon and argon at 16.6 eV and 11.5 eV are the result of collisions of slow thermal electrons with the excited atoms (the third reaction in (36)). The small peak in the oxygen argon mixture near 4 eV is probably due to electron detachment from negative oxygen ions. The energetic electrons from the detachment have energy of 3.6 eV. Thus, this simple device demonstrates the possibility of detection of the gas constituencies in the discharge plasma.

5. Conclusions

The practical measurement of EEDF has a half-century history. Since the first EEDF measurements in the 1960s, significant progress in EDF-measurement theory and technique, involving

a sophisticated analogue electronics and digital signal processing, has been achieved. Many new interesting features in the measured EEDF reflecting a variety of electron kinetic effects have been found in the last decades in different kinds of dc, pulsed and rf discharges.

However, the majority of EEDF measurements performed with homemade and commercial plasma probe equipment are of mediocre and even unacceptable quality because, in many works involving plasma probe diagnostics (and specifically in EEDF measurements), the basic requirements and limitation of classical probe diagnostics are ignored. Similarly, the issue of rf probe compensation in rf plasma diagnostics is frequently ignored or formally addressed with the application of some rf filter whose filtering function is inadequate. In many cases, a lack of skill with analogue electronics and rf techniques prevents obtaining the correct electrical measurements.

Therefore, the goal of this review is to increase awareness of the problems pertaining to the relationship between the actual plasma parameters and the probe experiment design. Main sources of error in EEDF measurements, remedies to avoid EEDF distortions and examples of positive resolutions of the problems are presented here for different types of gas-discharge plasmas. We also introduce the reader to unconventional methods of electron-distribution diagnostics in collisional, magnetized and anisotropic plasmas that are still under development and remain a challenge for budding scientists.

Acknowledgments

This work was supported by the DOE OFES (Contract No DE-SC0001939), NSF (Grant No CBET-0903635) and AFOSR.

References

[1] Stark J, Retschinky T and Schaposchnikoff A 1905 *Ann. Phys., Lpz.* **323** 213
[2] Langmuir I and Mott-Smith H M 1924 *Gen. Electr. Rev.* **27** 449
Langmuir I and Mott-Smith H M 1924 *Gen. Electr. Rev.* **27** 538
Langmuir I and Mott-Smith H M 1924 *Gen. Electr. Rev.* **27** 616
Langmuir I and Mott-Smith H M 1924 *Gen. Electr. Rev.* **27** 762
Langmuir I and Mott-Smith H M 1924 *Gen. Electr. Rev.* **27** 810
[3] Mott-Smith H M and Langmuir I 1926 *Phys. Rev.* **28** 727
[4] Druyvesteyn M J 1930 *Z. Phys.* **64** 781
[5] Kagan Y M and Perel V I 1964 *Sov. Phys.—Usp.* **6** 767
[6] Chen F F 1965 *Plasma Diagnostic Techniques* ed R H Huddlestone and S L Leonard (New York: Academic) p 113
[7] Medicus G 1967 *Invited Paper at 8th Int. Conf. Phenomena Ionized Gases (Vienna, Austria)*
[8] Schott L 1968 *Plasma Diagnostics* ed W Lochte-Holtgreven (Amsterdam/New York: North-Holland/Wiley) p 674 chapter II
[9] Kozlov O V 1969 *An Electrical Probe in a Plasma* (Moscow: Atomizdat)
[10] Swift J D and Schwar M J R 1970 *Electrical Probes for Plasma Diagnostics* (London: Iliffe Books)
[11] Chung P L, Talbot L and Touryan K J 1975 *Electric Probes in Stationary and Flowing Plasma* (Berlin: Springer)
[12] Ivanov Y A, Lebedev Y A and Polak L S 1981 *Methods of Contact Diagnostics in Non-Equilibrium Plasma-Chemistry* (Moscow: Nauka)
[13] Cherrington B E 1982 *Plasma Chem. Plasma Process.* **2** 113
[14] Amemija H and Sakamoto Y 1985 *J. Vac. Soc. Japan* **28** 177
[15] Hutchinson I H 1987 *Principles of Plasma Diagnostics* (New York: Cambridge University Press)
[16] Alekseev B V and Kotelnikov V A 1988 *Probe Method for Plasma Diagnostics* (Moscow: Energoatomizdat)
[17] Hershkowitz N 1989 *Plasma Diagnostics* vol 1 (Boston: Academic) p 113
[18] Stangeby P C 1989 *Plasma Diagnostics* vol 2 (Boston: Academic) p 157
[19] Godyak V A 1990 *Plasma–Surface Interaction and Processing of Materials* (Deventer: Kluwer) p 95
[20] Matthews G F 1994 *Plasma Phys. Control. Fusion* **36** 1595
[21] Demidov V I, Kolokolov N B and Kudryavtsev A A 1996 *Probe Methods for Low-Temperature Plasma Investigation* (Moscow: Energoatomizdat)
[22] Tichy M, Kudrna P, Behnke J F, Csambal C and Klagge S 1997 *J. Physique* IV **7** 397
[23] Amemiya H 1999 *Diagnostics of Ionized Gas* (Saitama: The Institute of Physical and Chemical Research (RIKEN))
[24] Ovsyannikov A A and Zhukov M F (ed) *Plasma Diagnostics* 2000 (Cambridge: Cambridge International Science)
[25] Demidov V I, Ratynskaia S V and Rypdal K 2002 *Rev. Sci. Instrum.* **73** 3409
[26] Chen F F 2003 *Mini-Course on Plasma Diagnostics* (*Lecture Notes on Langmuir Probe Diagnostics*) (*IEEE-ICOPS Meeting, Jeju, Korea*)
[27] Pfau S and Tichy M 2008 *Low Temperature Plasmas: Fundamentals, Technologies and Techniques* ed R Hippler *et al* (Berlin: Wiley) p 131
[28] Kolobov V I 2006 *J. Phys. D: Appl. Phys.* **39** R487
[29] Golubovskii Y B, Kolobov V I and al-Havat 1988 *Sov. Phys.—Tech. Phys.* **33** 1046
[30] Demidov V I, Kolokolov N B, Mezentsev A P and Mustafaev A S 1986 *Sov. J. Plasma Phys.* **12** 866
[31] Gill P and Webb C E 1977 *J. Phys. D: Appl. Phys.* **10** 299
[32] Kolokolov N B and Blagoev A B 1993 *Phys.—Usp.* **36** 152
[33] Morgulis N D and Kravchenko A I 1975 *Sov. Phys.—Tech. Phys.* **20** 848
[34] Amemiya H 1988 *J. Phys. Soc. Japan* **57** 887
[35] Amemiya H 1990 *J. Phys. D: Appl. Phys.* **23** 999
[36] Popov T and Petkov I 1998 *Vacuum* **51** 89
[37] Boedo J, Gray D, Chousal L, Conn R, Hiller B and Finken K H 1998 *Rev. Sci. Instrum.* **69** 2663
[38] Katsumata I and Okazaki M 1967 *Japan J. Appl. Phys.* Part 1 **6** 123
[39] Demidov V I, Koepke M E and Raitses Y 2010 *Rev. Sci. Instrum.* **81** 10E129
[40] Katsumata I 1996 *Contrib. Plasma Phys.* S **36** 73
[41] Demidov V I, Ratynskaia S V and Rypdal K 1999 *Rev. Sci. Instrum.* **70** 4266
[42] Ratynskaia S V, Demidov V I and Rypdal K 2000 *Rev. Sci. Instrum.* **71** 1367
[43] Demidov V I, Finnegan S M, Koepke M E and Reynolds E W 2003 *Rev. Sci. Instrum.* **74** 4558
[44] Demidov V I, Finnegan S M, Koepke M E and Reynolds E W 2004 *Contrib. Plasma Phys.* **44** 689
[45] Gunn J P, Devynck P, Pascal J-Y, Adamek J, Duran I, Hron M, Stockel J, Zacek F, Barina O and Hrach R 2002 *Czech. J. Phys.* **52** 1107
[46] Adamek J *et al* and the ASDEX Upgrade Team 2010 *Contrib. Plasma Phys.* **50** 854

[47] Shkarofsky I P, Johnston T W and Bachinski M P 1966 *The Particle Kinetics of Plasmas* (London: Addison-Wesley)
[48] Schoenberg K F 1979 A study of the general plasma characteristics of a high power multifilament ion source *PhD Thesis* (Lawrence Berkeley Laboratory)
[49] Schoenberg K F 1980 *Rev. Sci. Instrum.* **51** 1159
[50] Lieberman M A and Lichtenberg A J 2005 *Principles of Plasma Discharges and Materials Processing* (New York: Wiley)
[51] Godyak V A, Piejak R B and Alexandrovich B M 2002 *Plasma Sources Sci. Technol.* **11** 525
[52] Volkova L M, Devyatov A M, Kralkina E A, Sedov N N and Sherif M A 1975 *Vestn. Mosk. Univ., Fiz. Astron.* **16** 502
[53] Waymouth J F 1966 *J. Appl. Phys.* **37** 4492
[54] Little R G, Waymouth J F 1966 *Phys. Fluids* **9** 801
[55] Piejak R B, Godyak V A and Alexandrovich B M 1992 *Plasma Sources Sci. Technol.* **1** 179
[56] Kudryavtsev A A, Demidov V I, DeJoseph C A Jr, Adams S F and Serditov K Yu 2009 *Contrib. Plasma Phys.* **49** 373
[57] Godyak V A and Piejak R B 1990 *Phys. Rev. Lett.* **65** 996
[58] Godyak V A, Piejak R B and Alexandrovich B M 1992 *Phys. Rev. Lett.* **68** 40
[59] Godyak V A and Piejak R B 1993 *Appl. Phys. Lett.* **63** 3137
[60] VGPS Probe System www.plasmasensors.com
[61] Godyak V A and Maximov V N 1977 *Vestn. Mosk. Univ. ser. Fiz.* **6** 51
[62] Godyak V A and Alexandrovich B M 2005 *Proc. 27th ICPIG*, vol 1, ed T Goto (Eindhoven: The Nederland) p 221
[63] Godyak V A, Nagorny V I and Lee D S 2009 *GEC 2009* (*Saratoga Springs, NY*) (see also in [36])
[64] Godyak V A and Popov O I 1977 *Sov. Phys.—Tech. Phys.* **22** 461
[65] Godyak V A and Oks S N 1979 *Sov. Phys.—Tech. Phys.* **24** 784
[66] Paranjpe A P, McVittie J P and Self S A 1990 *J. Appl. Phys.* **67** 6718
[67] Flender U, Nguyen Thi B H, Wiesemann K, Khromov N A and Kolokolov N B 1996 *Plasma Sources Sci. Technol.* **5** 61
[68] Godyak V A 2011 *Plasma Sources Sci. Technol.* **20** 025004
[69] Cantin A and Gagne R R J 1974 *3rd Int. Conf. on Gas Discharges* (*London, UK*) p 625
[70] Braithwaite N S, Benjamin N M P and Allen J E 1987 *J. Phys. E: Instrum.* **20** 1046
[71] Nolle V L, Goodyear A, Hopgood A A, Picton P D and Braithwaite N St J 2002 *Knowl. Based Syst.* **15** 349
[72] Godyak V A and Piejak R B 1990 *J. Appl. Phys.* **68** 3157
[73] Godyak V A and Piejak R B 1993 *Appl. Phys. Lett.* **63** 3137
[74] Tsendin L D 1995 *Plasma Source Sci. Technol.* **4** 200
[75] Kolobov V I and Godyak V A 1995 *IEEE Trans. Plasma Sci.* **23** 503
[76] Kortshagen U, Bush C and Tsendin L D 1996 *Plasma Source Sci. Technol.* **5** 1
[77] Godyak V A and Khanneh A S 1986 *IEEE Trans. Plasma Sci.* **14** 112
[78] Godyak V A 2003 *Plasma Phys. Control Fusion* **45** A399
[79] Godyak V A, Piejak R B, Alexandrovich B M and Smolyakov A I 2000 *Plasma Sources Sci. Technol.* **9** 541
[80] Godyak V A and Alexandrovich B M 2004 *Appl. Phys. Lett.* **84** 1468
[81] Godyak V A and Alexandrovich B M and Kolobov V I 2001 *Phys. Rev.* E **64** 026406
[82] Godyak V A and Sternberg N 1991 *Proc. 20th ICPIG* vol 2 ed V Palleschi and M Vaselli (*Il Ciocco, Italy*) p 661
[83] Godyak V and Sternberg N 1990 *Phys. Rev.* A **42** 2299
[84] Maresca A, Orlov K and Kortshagen U 2002 *Phys. Rev.* E **65** 056405
[85] Rayment S W and Twiddi N D 1969 *Brit. J. Appl. Phys.* D **2** 1747
[86] Alexandrovich B M, Godyak V A and Lister G G 2004 *Proc. of the 10th Int. Symp. on Science and Technology of Light Sources* ed G Zissis (*Toulouse, France*) p 283
[87] Biondi M A 1954 *Phys. Rev.* **93** 1136
[88] Dovzhenko V A, Ershov A P and Solntsev G S 1974 *Sov. Phys.—Tech. Phys.* **19** 538
[89] Ershov A P, Dovzhenko V A and Solntsev G S 1977 *Vestn. Mosk. Univ., Fiz.* **6** 25
[90] Vasil'eva I A 1974 *High Temp.* **12** 409
[91] Ershov A P, Dovzhenko V A, Kuzovnilov A A and Oks S N 1981 *Sov. J. Plasma Phys.* **7** 334
[92] Godyak V A, Piejak R B and Alexandrovich B M 1993 *J. Appl. Phys.* **73** 3657
[93] Sudit I D and Woods R C 1994 *J. Appl. Phys.* **76** 4488
[94] Ivanov Y A, Lebedev Y A, and Polak L S 1977 *Phys. Plasma* **3** 146
[95] Asvadurov K D and Vasil'eva I A 1975 *Sov. Phys.—Tech. Phys.* **20** 996
[96] Demidov V I, Ratynskaia S V and Rypdal K 2001 *Rev. Sci. Instrum.* **72** 4106
[97] Klagge S 1975 *Beitr. Plasmaphys.* **15** 309
[98] Thomas T L and Battle E L 1970 *J. Appl. Phys.* **41** 3428
[99] Rayment S W and Twiddy N D 1973 *J. Phys. D: Appl. Phys.* **6** 2242
[100] Godyak V A 2005 *Phys. Plasmas* **12** 055501
[101] Godyak V A, Kasouit S and Bulkin P, to be published
[102] Roca i Cabarrocas P, Bulkin P, Daineka D, Dao T H, Leempoel P, Descamps P, Kervyn de Meerendr T and Charliac J 2008 *Thin Solid Films* **516** 6834
[103] Fox-Lion N, Metzler D, Oehrlein G S and Godyak V A, to be published
[104] Demidov V I and Kolokolov N B 1981 *Sov. Phys.—Tech. Phys.* **26** 533
[105] Hannemann M 2008 *Contrib. Plasma Phys.* **48** 446
[106] Amemiya H 1976 *Japan J. Appl. Phys.* **15** 1767
[107] Demidov V I 1983 *Int. J. Electron.* **54** 183
[108] Demidov V I, Kolokolov N B and Toronov O G 1984 *Sov. Phys.—Tech. Phys.* **29** 230
[109] Blagoev A B, Demidov V I, Kolokolov N B and Toronov O G 1981 *Sov. Phys.—Tech. Phys.* **26** 1179
[110] Volkova L M, Demidov V I, Kolokolov N B and Kral'kina E M 1984 *High Temp.* **22** 612
[111] Demidov V I and DeJoseph C A Jr 2005 *Rev. Sci. Instrum.* **76** 086105
[112] Waldmann O and Fussmann G 2008 *Contrib. Plasma Phys.* **48** 534
[113] Lobbia R B and Gallimore A D 2010 *Phys. Plasmas* **17** 073502
[114] Swift J D 1962 *Proc. Phys. Soc. Lond.* **79** 697
[115] Lukovnikov A I and Novgorodov M Z 1971 *Brief Communications Physics* #1, 27
[116] Golubovsky Y B, Zakharova V M, Pasunkin V I and Tsendin L D 1981 *Sov. J. Plasma Phys.* **7** 340
[117] Popov Tsv. K, Dimitrova M, Dias F. M, Tsaneva V N, Stelmashenko N A, Blamire M G and Barber Z H 2006 *J. Phys. Conf. Ser.* **44** 60
[118] Popov T K, Dimitrova M and Dias F M 2004 *Vacuum* **76** 417
[119] Gorbunov N A, Kolokolov N B and Latyshev F E 2001 *Tech. Phys.* **46** 391
[120] Arslanbekov R R, Khromov N A and Kudryavtsev A A 1994 *Plasma Sources Sci. Technol.* **3** 528
[121] Malkov M A 1991 *High Temp.* **29** 329
[122] Demidov V I, Ratynskaia S V, Rypdal K and Armstrong R J 1999 *Phys. Plasmas* **6** 350
[123] Rypdal K, Grønvoll E, Øynes F, Fredriksen Å, Armstrong R, Trulson J and Pécseli H L 1994 *Plasma Phys. Control. Fussion* **36** 1099
[124] Popov T K, Ivanova P, Stöckel J and Dejarnac R 2009 *Plasma Phys. Control. Fussion* **51** 065014

[125] Popov T K, Ivanova P, Dimitrova M, Kovačič J, Gyergyek T and Čerček M 2011 *Plasma Sources Sci. Technol.* **20** at press
[126] Kagan Y M, Lavrov B P and Lyaguschenko R I 1977 *Sov. Phys.—Tech. Phys.* **22** 349
[127] Abroyan M A, Demidov V I, Kagan Y M, Kolokolov N B and Lavrov B P 1975 *Opt. Spectrosc.* **39** 12
[128] Mezentsev A P and Mustafaev A S 1985 *Sov. Phys.—Tech. Phys.* **30** 1319
[129] Mezentsev A P, Mustafaev A S and Fedorov V L 1998 *Electron Kinetics and Applications of Glow Discharges* ed U Kortshagen and L D Tsendin (New York: Kluwer) p 531
[130] Fedorov V L 1985 *Sov. Phys.—Tech. Phys.* **30** 584
[131] Woods R C and Sudit I D 1994 *Phys. Rev.* E **50** 2222
[132] Lapshin V F and Mustafaev A S 1989 *Sov. Phys.—Tech. Phys.* **34** 150
[133] Mezentsev A P, Mustafaev A S and Fedorov V L 1988 *J. Phys. D: Appl. Phys.* **21** 1464
[134] Lapshin V L, Mezentsev A P and Mustafaev A S 1989 *J. Phys. D: Appl.Phys.* **22** 857
[135] Demidov V I and Kolokolov N B 1987 *Sov. Phys. J.* **30** 97
[136] Volkova L M, Demidov V I, Kolokolov N B and Kralkina E A 1983 *Sov. Phys.—Tech. Phys.* **28** 583
[137] Demidov V I, Adams S F, Blessington J, Koepke M E and Williamson J M 2010 *Contrib. Plasma Phys.* **50** 808